The statistical analysis of wildfire growth

Harry Podschwit

A dissertation

submitted in partial fulfillment of the

requirements for the degree of

Master of Science

University of Washington

2017

Reading Committee:

Peter Guttorp, Chair

E. Ashley Steel

Narasimhan K. Larkin

Program Authorized to Offer Degree:

Quantitative Ecology and Resource Management

University of Washington

Abstract

The statistical analysis of wildfire growth

Harry Podschwit

Chair of the Supervisory Committee:
Professor Emeritus, Peter Guttorp.
Statistics

Understanding and quantifying wildfire behavior is of interest to the scientific community, as well as public health and fire management professionals. To achieve this end, there is a demand for statistical descriptions of wildfire behavior and its relationship to the environment. However, wildfire behavior can be complex, described by multiple characteristics such as final size, duration and growth rates, and influenced by processes that can be regionally dependent. Further challenges arise due to the poor quality and availability of cumulative burn area time series data, which often contain missing and erroneous measurements. To address these issues, a variety of methods are presented. Multiple wildfire behaviors are represented using a simple decomposition of cumulative burn area time series that measures four meaningful quantities from the growth curve. The relationship between wildfire activity and the environment are approximated using

regionally specific generalized linear models. Weather and landscape data are used to predict various measures of wildfire behavior. Validation results suggested that most of the models generalized well to independent data, and have potentially useful applications in climatological research. Data quality issues common to cumulative burn area time series are addressed using Bayesian state-space models, which reconstruct growth curves from multiple corrupted burn area time series. Two state space models are presented, a stationary version that assumes idealized fire growth, and a non-stationary version that produces reconstructions with time-varying growth rates. The relative computational costs and goodness-of-fit is illustrated by reconstructing the growth curves of 13 wildfires from 2014 wildfire season using growth data coming from two sources, fire perimeters from the Geospatial Multi-Agency Coordination (GeoMAC) and cumulative hotspot detects from the Hazard Mapping System (HMS). The stationary model had minimal computational costs, but rarely produced adequate descriptions of the burn area observations. The non-stationary model had much higher computational costs, but produced realistic estimates of the time series. An informal sensitivity analysis suggested that the reconstructed curves would be robust to changes in the priors. The main application of the state-space models is to reconstruct burn area time series, which can in turn be used for statistical analysis or validation of currently existing growth models. The framework can be modified for other purposes as well including forecasting burn area, and predicting the extinguishment date of a fire.

TABLE OF CONTENTS

LIST OF FIGURES

LIST OF TABLES

ACKNOWLEDGEMENTS

I would like to give an additional thanks to Eli Holmes, Eric Ward and Mark Schuerell who introduced me to the concept of state space modeling and gave helpful feedback early into this research. I would also like to thank Ernesto Alvarado, Ashley Blazina, Paulina Llamas Casillas, Fabiola Chavez, William Chen, Colton Miller, Cole Monahan, Kiva Oken, Susan O'Neil and Brian Potter for their input and encouragement. This research could not have been possible without the support of the Northwest Climate Science Center, the Quantitative Ecology and Resource Management program. I would like to close by extending my fullest gratitude to my advisors, Peter Guttorp, Narasimhan Larkin, and Ashley Steel, who have profoundly and consistently helped my technical and professional development for past couple years.

Chapter 1. INTRODUCTION

Understanding the drivers of wildfire activity is of interest to a variety of scientists, as well as wildfire managers and policy makers. Fires are a key successional phenomenon in many ecosystems (Koniak 1985, Gunderson and Snyder 1994, Minnich and Bahre 1995) and can profoundly influence hydrological (Elliot et al. 2005), soil (Johansen et al. 2001) and ecological (Nelle et al. 2000) processes. Fires also have serious socio-economic impacts (Morton et al. 2003) like road closures, evacuations, loss in property values and damage to view sheds. Wildfires also pose risks to human health, which can come directly result from the flames, or indirectly through smoke impacts which can impact health hundreds of miles away from the fire (Moeltner et al. 2013). Given that climate change is expected to change global fire regimes in various ways (Flannigan et al. 2009, Moritz et al. 2012), there is an increasing demand to understand fires and how their behavior is related to environmental conditions. Quantifying relationships between environmental conditions and wildfire behavior allow better prediction of, and planning for, changes to future wildfire regimes. However, quantifying relationships between the environment and wildfire behavior is complicated due to the variety of measurements that potentially represent wildfire behavior. Fire size, duration and rate-of-spread measurements all communicate information concerning the severity of a fire, but also describe unique characteristics of its growth. Further, independent processes may control each measurement of wildfire activity and it cannot be assumed that any hypothetical change to the environment or landscape would alter each measurement in the same way (Fischer et al. 2015). Hence, fully understanding future wildfire patterns will require using multiple measurements of

wildfire behavior, and quantifying how environmental changes can alter each of the measurements.

In this introduction, I will present commonly used wildfire behavior measurements and discuss their importance to scientific research, fire fighting operations, and land management. A brief review of the wildfire modeling will be presented to describe the tools that currently exist to quantify the relationship between the environment and wildfire behaviors, and motivate the use of statistical models. The discussion of statistical modeling will transition into a presentation of the potential sources of cumulative burn area time series for wildfires in the United States, as well as their benefits and limitations. I will close the introductory chapter with a summary of mathematics that will be required to understand the tools and results developed in this manuscript.

1.1 MEASURING WILDFIRE BEHAVIOR

Wildfires are a complex process that can be measured using a variety of measurements, each capturing a unique dimension its overall behavior. Fire occurrence, is perhaps the simplest example, describing incidents as a binary presence/absence variable. That is, when and where is there burning on the landscape. Wildfire presence can broadly describe the location, time and place of an incident (Taylor et al. 2013) or provide detailed descriptions of actively burning locations across the landscape (Csiszar et al. 2006). Presence-absence measures are commonly used to count the frequency of wildfires if they are recorded consistently over time and space. Although the simplicity of presence-absence measurement is appealing and useful for measuring wildfire frequency, it can mask important information about how wildfire behavior. Presence-absence descriptions do not describe the final burn area or duration of an individual wildfire event, both of which can be potentially important information to scientists (Van der Werf et al.

2006), fire managers (Thompson 2013), and health professionals (Moeltner et al. 2013). Given these limitations and that nearly all fire metrics will be conditional on fire occurrence, more detailed measurements of wildfire behavior are commonly used.

The next level of detail concerns the final burn area, which describes incidents by the size it grew to when it was extinguished. This measurement can be described on a continuous scale (Turetsky et al. 2004) or categorically, large or very-large burn area groups for example (Barbero et al. 2014). Final burn area is perhaps the most commonly used measurement of wildfire activity by researchers and requires relatively little data. Measurements can come from a variety of different sources from crude field-estimates (Kasischke et al. 2002) to estimates based on satellite imagery (Eidenshink et al. 2007). Unlike other measurements, only one post-fire estimate of burn area is needed to calculate final burn area. The definition of final burn area is seemingly straightforward, but there is inherent subjectivity in the classification of burned regions and disagreement between data sources is common. For example, a burn area observation may reflect the true physical area burned by the fire and exclude unburned interior patches. This quantity is sometimes referred to as the blackened area of a fire. On the other hand, burn area observations may be of the affected area of the fire and map the perimeter of the fire only, ignoring unburned interior regions. These distinctions are important because the affected area could be more than 1.5 times larger than the blackened area. Estimates of burn area are further clouded by observation errors, which are common in burn area data. Observation errors arise for a variety of reasons including poor fire detection, human error, topography, and safety issues (Kolden et al. 2012). Burn area measurements are used for a variety of purposes including estimating wildfire emissions (Van der Werf et al. 2006), quantifying smoke related health impacts (Moeltner et al. 2013), and predicting firefighting costs (Gebert et al. 2007).

Another commonly used measurement is wildfire duration, which can have multiple definitions. Duration can be the time from the fire's ignition until further spread is unlikely (Dowdy and Mills 2012), the number of consecutive days of hotspot detection (Hernandez et al. 2015_a), days between start and end dates of fire reports (Keeley et al. 2009) or based on percent of final size (Larkin et al. 2015). Given that the final burn area is often repeated multiple times near the end of the fire's lifetime, estimates of wildfire duration will change depending on the how it is measured (Filippi et al. 2014). Given the multiple methods of measuring duration and the additional information requirements, it is less commonly used than final burn area, although a number of analyses have included duration (Thompson 2013, McKenzie et al. 2006, Khabarov et al. 2008, Fried et al. 2006, Scott and Thompson 2014, Keeley et al. 2009, Braun et al. 2010, Van Wagtendonk and Lutz 2007, Dowdy and Mills 2012, Hernandez et al. 2015_a). Measurements of duration are important to calculating suppression costs of individual wildfires (Thompson 2013) and quantifying the health effects of smoke (Mirabelli et al. 2009).

Measurements of spread are an important quantity that can be calculated in multiple ways. Rate of spread (ROS) measures the rate at which heat transfers from burned to unburned material (Taylor et al. 2013) and is often included in fire reports and case studies (Taylor and Williams 1968, Anderson 1968, Cheney et al. 2012). ROS is sensitive to weather and landscape conditions, and can be highly variable in space and time. Hence, field estimates of ROS may not be representative of the ROS over the entire burning perimeter of the fire (Taylor et al. 2013). Daily area burned time series are an alternative measure of spread (Billmire et al. 2014, Birch et al. 2014) and maximum daily area burned measurements are particularly important in both chapters of this manuscript. Qualitative measures of growth, like high- and low-spread days, have also been used (Finney et al. 2009). Rate of spread measurements are often used throughout

wildfire suppression operations and are important to predict to firefighter safety (Alexander and Thomas 2003). Moreover, daily area burned measures can be helpful in understanding the post-fire effects on vegetation (Birch et al. 2014), and measuring smoke related health effects (Moeltner et al. 2013).

In addition to these quantitative growth measures, qualitative measurements are broadly applicable and have been used to describe various behaviors, e.g. crowning (Cruz et al. 2004), ignition method (Van Wagtendonk and Lutz 2007), and predominant atmospheric conditions (Brotak and Reifsnyder 1977). These measures of wildfire behavior capture important aspects of a fire's growth and can be used to approximate the complex, multi-dimensional of wildfire activity.

1.2 MODELING WILDFIRE BEHAVIOR

Wildfire growth models are another important way of summarizing wildfire behavior and relating it to the environment. Growth models can be constructed using a variety of techniques that can be broadly divided into physical and statistical methods. The earliest physical models of wildfire activity go back to (Fons 1946) and at least 40 physical/semi-physical models of fire spread, and as many as 30 statistical models of spread have been published since. ROS models input environmental and landscape data to estimate the one-dimensional linear progression of the flaming edge of a fire. The estimates of ROS can be fed into fire growth models to estimate burn area in two dimensions (Taylor et al. 2013), which can be as simple as elliptical models of fire growth (Van Wagner 1969) to complex simulations like FARSITE, that require spatially explicit maps of fuel and topography, as well as detailed information about the weather (Finney 2004). In addition to FARSITE, there are more than 40 different wildfire growth models that have been developed since 1969. Unfortunately, the data inputs required for simulations may be onerous,

and the models can be sensitive to changes in inputs, and may not be thoroughly validated (Taylor et al. 2013). Moreover, spatially explicit progression maps are not always necessary and it is often sufficient to model the measurements of wildfire behavior.

A number of the wildfire behaviors measurements described in the previous section have been modeled quite well using statistical models. Burn area distributions are commonly assumed to follow power law-like behaviors, suggesting the use of Pareto type distributions (Schoenberg et al. 2003); however, other distributions like the Gamma (Hernandez et al. 2015_b) have also been used. Wildfire duration has been modeled using Markov Chains (Thompson 2013), linear (McKenzie et al. 2006) and quadratic (Khabarov et al. 2008) models, and simulations (Fried et al. 2006, Scott and Thompson 2014), and empirical distributions (Keeley et al. 2009, Braun et al. 2010, Van Wagtendonk and Lutz 2007, Dowdy and Mills 2012). Containment probabilities have been related to various fuel types, suppression and other covariates using mixed modeling (Finney et al. 2009). Hence, there is a great variety of modeling techniques that have been used to describe wildfire behavior, ranging from theoretical physics based models of fire growth to statistical models of aggregate measurements of wildfire behavior. However, one of the challenges to adopting these statistical techniques is related to issues with quality and quantity of cumulative burn area data (Taylor et al. 2013, Kolden et al. 2012)

1.3 CUMULATIVE BURN AREA DATA

Statistical wildfire growth modeling often requires measurements of cumulative burn area taken over a fire's lifetime. The data can be extracted from a variety of sources that include non-spatial reports and spatially explicit burn perimeters. In the United States, a popular source of non-spatial burn area measurements is incident command system 209 (ICS-209) forms. These reports are distributed almost daily for large wildfires burning on federally owned lands in the

United States. They provide agency managers with a daily snapshot of wildfire activity, and are used for decision making and planning at broader geographic scales. Each individual report contains 47 blocks of information including date, time, coordinates, management strategy, fuels, values-at-risk, ignition dates, expected containment dates, and fire size (Thompson 2013). The quality of the fire size estimates can vary, even throughout the lifetime of an individual incident. Burn area estimates can be based approximate ground-based best guesses, ground and aerial GPS information, and imagery from fixed-wing and satellite platforms. The data quality of these reports can change over a fires lifetime, and reductions in burn area may be reported when better mapping technology becomes available. Written wildfire reports can also be found through some state and local agencies (Short 2014). Whatever the case, these non-spatial reports can be used to generate, at least partial, time series of cumulative burn area observations throughout the fire's lifetime.

Spatially explicit fire perimeter maps can also be a rich source of burn area data. The Geospatial Multi-Agency Coordination (GeoMAC) produces wildfire perimeter data throughout some large fire's lifetime. These maps are produced for fire and land managers, the public, and researchers to provide the latest information of wildfire progression. Fire perimeter maps are constructed from a variety of data sources. Perimeters may be mapped using field-based methods that use GPS to traverse the boundaries via foot, land-vehicle or aircraft. Maps can also be constructed using infrared imagery collected from satellite or aircraft (Walters 2008). These maps can also be produced using other information including field-based intelligence, interpretation of aerial photography (Parks 2014, Kasischke et al. 2002), and by estimating burn area from satellite hotspot detects (Veraverbeke et al. 2014, Parks 2014). Burn area estimates derived from satellite hotspot data can have problems with accuracy, but are recorded

consistently and globally, and are useful when burn scar data is unavailable (Zhang et al. 2011). Hence, spatially explicit burn area maps and written reports are produced from a variety of sources, and can be used to generate cumulative burn area time series, which can be used to calculate important measurements of wildfire activity, validate models of wildfire behavior and other important tasks to scientists and fire managers. As will be presented in this manuscript, detailed fire information can be described and related to the environment by using simple mathematical models of growth, and decomposing the burn area time series into meaningful wildfire behavior measurements. In the next section, I will present the mathematics that will be required to sufficiently describe the modeling approaches used in this manuscript.

1.4 BACKGROUND MATHEMATICS

1.4.1 *Mathematical models of growth*

The best mathematical model of fire growth will capture important aspects of a fire's behavior and size. Before ignition, a fire has a size of zero fire. After ignition, the fire will continue to grow as long as the flame front produces sufficient heat to ignite the adjacent biomass, living or dead. This process continues until the fire eventually reaches its final size (Taylor et al. 2013). One simple representing the process in continuous time is to assume a logistic differential equation.

$$\frac{dX}{dt} = rX(1 - {}^{X}/_{K}).$$

This model is controlled by two parameters referred to as the inherent growth parameter, r, and the final burn area, K. In addition, initial conditions must be imposed and setting $\mathrm{X}(0) = X_0$ is popular choice, leading to the analytic solution of

$$X(t) = KX_0/(X_0 + (K - X_0)e^{-rt}).$$

However, since most burn area data is typically recorded at a daily time-scale, a discrete time alternative to this model may be more appropriate. However, two difference equation models can be interpreted as being the discrete-time interpretation of the logistic differential equation: the logistic map and the Beverton-Holt difference equation.

The logistic map is written as,

$$X(t+1) = rX(t)(1 - X(t)).$$

For intermediate values of r, between 1 and 3, the solutions approach $(r-1)/r$ and will have a S-shaped curve. If r becomes too large, pathologies that are inconsistent with wildfire growth, decreasing burn area and chaos, begin to arise. The logistic map's model structure is direct analog to the nondimensionalized logistic differential equation (Murray 2002). However, given the models instability, it will not be considered further.

The other discrete time logistic model is the Beverton-Holt difference equation.

$$X(t+1) = e^r KX(t)/(K + (e^r - 1)X(t)).$$

This Beverton-Holt model can be solved analytically by applying $Y(t+1) = 1/X(t+1)$ and reverse transforming. The model is identified as the logistic model because the solution is interpolated by the continuous-time logistic differential equation. For $r < 0$, the model decays to zero. For $r > 0$, it approaches the final burn area K (Kot 2001). It should be noted that other logistic like growth models, such as the Gompertz model (Winsor 1932), could also have been considered.

1.4.2 *Generalized linear models*

One flexible method of relating wildfire behavior measurements to environmental covariates is through the use of generalized linear models (GLMs). GLMs are statistical models requiring two components: a response and link function. The response is a probability

distribution function from the exponential family that describes the conditional distribution of models response. The link function relates the linear combination of covariates to the model mean.

$$g(\mu) = \beta_0 + \beta_1 x_1 + \cdots + \beta_p x_p.$$

The gamma with log link, beta with logit link and negative binomial with log link will be the three model configurations used in this manuscript.

The gamma distribution is a flexible distribution for continuous skewed responses that are strictly greater than zero. The gamma distribution has the probability density function.

$$f(y) = \frac{1}{\Gamma(\nu)} \lambda^{\nu} y^{\nu-1} e^{-\lambda y}.$$

The model mean is $\mu = \nu/\lambda$, with model variance $\frac{\mu^2}{\nu} = \nu/\lambda^2$, the former being controlled by the linear combination of covariates and latter controlled by ν. The log link implies that the effect of the predictors is multiplicative on the mean. Skewed continuous data can also be modeled using an inverse Gaussian response (Faraway 2006).

The beta distribution is a flexible distribution that supports random variables on the unit interval, such as percentages, and has the probability density function.

$$f(y) = \frac{1}{B(\alpha,\beta)} x^{\alpha-1}(1-x)^{\beta-1}.$$

Here the model mean is $\mu = \alpha/(\alpha+\beta)$ and model variance $\frac{\alpha\beta}{(\alpha+\beta)^2(\alpha+\beta+1)} = \mu(1-\mu)/(1+\phi)$. Again the response is controlled by the linear combination of covariates through $\mu = \alpha/(\alpha+\beta)$ and variance through the scale parameter ϕ. The logit link suggests that the effects of the predictors are multiplicative on the ratio of response and its complement (Ferrari and Cribari-Neto 2004).

Lastly, the negative binomial response with a log link will be used for count data in this manuscript and has probability mass function.

$$f(y) = \binom{y + r - 1}{y} (1 - p)^r p^y.$$

Here $E[Y] = \mu = pr/(1 - p)$ and $Var[Y] = \frac{pr}{(1-p)^2} = \mu + \mu^2/\phi$. Strictly speaking, the negative binomial is not in the exponential family but is close enough in form to use GLM. Maximum likelihood estimates must be calculated by iteratively estimating model coefficients and ϕ. The Poisson distribution could also have been used, but the negative binomial is particularly appropriate when the variance that is larger than the mean (Hilbe 2011).

1.4.3 *Model selection and validation*

There is often a need to select a best model from a suite of competing models and for this a variety of selection methods have been developed. In some cases, the best model is the one with the highest probability of being the true model and the goal is model identification. Alternatively, the best model may be defined as the one that optimizes a loss function, and the goal is model estimation. Since it is oftentimes assumed that no true model exists, estimation is a more generally applicable criterion. When estimation is the goal, an easily interpretable method of model selection is to choose the model with the minimum prediction error. Prediction error can be estimated by calculating the loss based on the same data that trained the models, however, this will lead to overly optimistic error estimates and risks overfitting. It is therefore prudent to estimate prediction error using data that was not used to fit the models. This is commonly done using the simple holdout method, which divides the data into two mutually exclusive groups. One group is used to fit the models, and the other group contains the remaining data, and is used to estimate the prediction error. This model selection algorithm can seemingly be applied to

nearly any model due to the universality of data splitting procedures (Arlot and Celisse 2010). The single split holdout uses one partition for both selection and assessing prediction error. Hence, prediction error estimates may also be overly optimistic in the simple holdout since the prediction error was optimized. When both quantities are of interest, then it is appropriate to use a three-way holdout. Here the data is split into three mutually independent sets. The first group is used for fitting the models, the second for model selection and the last for quantifying the error of the final model using independent data. The independent blocks of data prevent overly optimistic estimates of the prediction error that result from two-way holdouts and resubstitution (Dua and Chowriappa 2012).

1.4.4 *Bayesian Statistics*

Incorporate background information and evidence into the model building and fitting can be desirable when data is sparse. A natural way of doing this is through the use of Bayesian statistics. Bayesian statistics interpret probabilities to represent the strength in model parameters. The alternative is to the Bayesian paradigm is frequentist statistics, which interpret probabilities to represent the frequency in which certain events should be expected to occur. Bayesian statistics define the probabilities of model parameters using Bayes theorem,

$$p(\boldsymbol{\theta}|y) = \frac{p(y|\boldsymbol{\theta})p(\boldsymbol{\theta})}{p(y)}.$$

The probability of the vector of model parameters, $\boldsymbol{\theta}$, given the vector of observations, y, is called the posterior, $p(\boldsymbol{\theta}|y)$. The probability of the observations given the model parameters is called the likelihood, $p(y|\boldsymbol{\theta})$. The background information is incorporated through the prior, $p(\boldsymbol{\theta})$, which is a probability distribution that represents the a priori belief in the model

parameters. The probability of the vector of observations, $p(y)$, is often omitted so the posterior is just written as,

$$p(\boldsymbol{\theta}|y)\ \alpha\ p(y|\boldsymbol{\theta})p(\boldsymbol{\theta}).$$

Oftentimes, the statistical model of interest is multivariate and complicated, making direct calculation of the posterior difficult or impossible. Hence, simulation methods have been developed to generate samples from the posterior distribution, from which statistics concerning the certainty in the model parameter can be calculated. In particular, Markov Chain Monte Carlo (MCMC) methods, which rely on Markov chains that explore and sample the posterior distribution, are applicable to a broad variety of problems and have become increasingly a popular in recent years.

Developments in statistical software have increased the accessibility of MCMC techniques to researchers outside of the statistical community. For instance, Just Another Gibbs Sampler (JAGS) and Bayesian Inference Using Gibbs Sampling (BUGS), input data and text files describing the model structure, and output samples from the posterior. Internally JAGS software converts the model formulation into a graphical representation. Variables are converted into nodes, which represent stochastic or deterministic relationships. The graphical representation of the model is sample by iterating through the stochastic nodes via Gibbs sampling (Plummer 2003). A single Gibbs sampling step will iterate through each of the stochastic nodes in the graph, and sequentially update the Markov chain. The Gibbs step ends after each parameter has been sampled. Each iteration occurring within a single Gibbs step samples a single parameter updated via a random draw from the conditional posterior. The updated vector of model parameters is returned at the end of each iteration and the next iteration will repeat the same process for the next model parameter in the sequence (Yildirim 2012).

MCMC sampling can be used to fit state-space models, which in general, cannot be done analytically. State-space models assume that the observations were generated from two model components, a process state and observation state. The process state components models the true process that is not directly measureable and imposes structure onto the data generating process. The observation state components models the data generating processes, which is based on the process state. The state space framework can be defined mathematically as,

$$x_t = f(x_{t-1}, \eta_t, \boldsymbol{\delta}).$$

$$y_t = h(x_t, \epsilon_t, \boldsymbol{\gamma}).$$

The first equation is the process equation, f, and x_t is the unobservable state. The process equation controls how the process state transitions through time. The second is the observation equation, h, and y_t are the data. The observation equation controls how x_t is related to the observations. The errors terms for the unobservable and observable states are respectively denoted, η_t and ϵ_t. The nuisance parameters are denoted, $\boldsymbol{\delta}$ and $\boldsymbol{\gamma}$, for the unobservable and observable states respectively. Although broadly applicable and easily interpretable, state-space models can be very difficult to fit. If the process is linear and the errors Gaussian, the Kalman filter can be used, however other techniques must be applied if the observations are non-Gaussian or the process is non-linear (Petris and Petrone 2011). State-space models can be fit using the MCMC techniques described earlier, which have the additional advantage of quantifying the uncertainty probabilistically and being applicable to variety of models. The posterior can be sampled by Gibbs sampling the conditional distributions $p(\boldsymbol{X}|\, \boldsymbol{Y}, \boldsymbol{\gamma}, \boldsymbol{\delta})$, $p(\boldsymbol{\gamma}|\, \boldsymbol{X}, \boldsymbol{Y}, \boldsymbol{\delta})$ and $p(\boldsymbol{\delta}|\, \boldsymbol{X}, \boldsymbol{Y}, \boldsymbol{\gamma})$, where the vector of observations is $\boldsymbol{Y} = \{y_0, y_1, \cdots, y_n\}$ and the vector process-states is $\boldsymbol{X} = \{x_0, x_1, \cdots, x_n\}$ (Geweke and Tanizaki 2001).

1.4.5 *Concluding remarks*

I will use the data and mathematical techniques introduced in this section to describe wildfire behaviors and their relationship to the environment. In Chapter 2, I will present a novel method of decomposing cumulative burn area time series into measurements of wildfire behaviors. I will apply this decomposition method to a large database of burn area time series and use these measurements to explore trends and patterns of wildfire behaviors across the Continental United States. Regionally specific models of wildfire behavior will be constructed based on weather and landscape data inputs. The best predictors of wildfire behaviors in each region will be identified by the coefficients of the best models, and seasonal trends inferred from historical model predictions. This general method may serve as a starting point for those interested in relating wildfire growth to other environmental variables, and the models themselves show potential to predict wildfire behaviors from climatological data.

In Chapter 3, I improve the way researchers deal with pathologies of missing and erroneous measurements that are typical in cumulative burn area datasets. To do this, I will use a state-space model to represent cumulative burn area time series. The unobservable process will describe the true cumulative burn area time series and will conform to prior knowledge of how wildfires grow over time, part of which is will be based on the results from Chapter 2. Satellite and ground based measurements of burn area will be modeled conditional on the unobservable process, allowing missing and erroneous data to be dealt with in a natural way. The state-space model is intended as a general tool for combining multiple burn area time series that may disagree about burn area measurements or occur on different scales, into a single realistic reconstruction. The reconstructed time series could be used to validate currently existing models,

as well as be used to calculate wildfire behavior measures that may otherwise be difficult to calculate from corrupted and incomplete burn area time series.

1.5 REFERENCES

Alexander ME, Thomas DA (2003) Wildland fire behavior case studies and analyses: Other examples, methods, reporting standards, and some practical advice. Fire Management Today, 63:4-12

Anderson HE (1968). Sundance Fire: an analysis of fire phenomena. Res. Pap. INT–56. Ogden, UT: USDA Forest Service, Intermountain Forest and Range Experiment Station.

Arlot S, Celisse A (2010). A survey of cross-validation procedures for model selection. Statistics surveys, 4, 40-79

Barbero R, Abatzoglou JT, Steel EA, Larkin NK (2014). Modeling very large-fire occurrences over the continental United States from weather and climate forcing. Environmental research letters, 9(12), 124009

Billmire M, French NH, Loboda T, Owen RC, Tyner M (2014). Santa Ana winds and predictors of wildfire progression in southern California. International Journal of Wildland Fire, 23(8), 1119-1129

Birch DS, Morgan P, Kolden CA, Hudak AT, Smith AM (2014). Is proportion burned severely related to daily area burned?. Environmental Research Letters, 9(6), 064011

Bradstock RA, Hammill KA, Collins L, Price O (2010). Effects of weather, fuel and terrain on fire severity in topographically diverse landscapes of south-eastern Australia. Landscape Ecology, 25(4), 607-619

Braun WJ, Jones BL, Lee JS, Woolford DG, Wotton BM (2010). Forest fire risk assessment: an illustrative example from Ontario, Canada. Journal of Probability and Statistics, 2010.

Brotak EA, Reifsnyder WE (1977). An investigation of the synoptic situations associated with major wildland fires. Journal of Applied Meteorology, 16(9), 867-870

Cheney NP, Gould JS, McCaw WL, Anderson WR (2012). Predicting fire behaviour in dry eucalypt forest in southern Australia. Forest Ecology and Management, 280, 120-131

Cruz MG, Alexander ME, Wakimoto RH (2004). Modeling the likelihood of crown fire occurrence in conifer forest stands. Forest Science, 50(5), 640-658

Csiszar IA, Morisette JT, Giglio, L (2006). Validation of active fire detection from moderate-resolution satellite sensors: the MODIS example in northern Eurasia. IEEE Transactions on Geoscience and Remote Sensing, 44(7), 1757-1764

Dowdy AJ, Mills GA (2012). Characteristics of lightning-attributed wildland fires in south-east Australia. International journal of wildland fire, 21(5), 521-524

Dua S, Chowriappa P (2012). Data mining for bioinformatics. CRC Press.

Eidenshink J, Schwind B, Brewer K, Zhu Z, Quayle B, Howard S (2007). A project for monitoring trends in burn severity. Fire Ecology 3 (1): 3-21. Fire Ecology Special Issue *Vol*, *3*, 4

Elliott JG, Smith ME, Friedel MJ, Stevens MR, Bossong CR, Litke DW, Bauer MA (2005). Analysis and mapping of post-fire hydrologic hazards for the 2002 Hayman, Coal Seam, and Missionary Ridge wildfires, Colorado.

Faraway JJ (2006). Extending the Linear Model with R: Generalized Linear. Mixed Effects and Nonparametric Regression Models, 1.

Ferrari S, Cribari-Neto F (2004). Beta regression for modelling rates and proportions. Journal of Applied Statistics, 31(7), 799-815

Filippi JB, Mallet V, Nader B (2014). Representation and evaluation of wildfire propagation simulations. International journal of wildland fire, 23(1), 46-57

Fischer MDLA, Di Bella CM, Jobbágy EG (2015). Influence of fuel conditions on the occurrence, propagation and duration of wildland fires: A regional approach. Journal of Arid Environments, 120, 63-71

Finney MA (2004). FARSITE: Fire area simulator: model development and evaluation. Ogden, UT: US Department of Agriculture, Forest Service, Rocky Mountain Research Station.

Finney MA (2007). A prototype simulation system for large fire planning in FPA. US Department of Agriculture, Forest Service, July, 5.

Finney MA, Grenfell IC, McHugh CW (2009). Modeling containment of large wildfires using generalized linear mixed-model analysis. Forest Science, 55(3), 249-255

Flannigan MD, Krawchuk MA, de Groot WJ, Wotton BM, Gowman LM (2009). Implications of changing climate for global wildland fire. International journal of wildland fire, 18(5), 483-507

Fons WL (1946). Analysis of fire spread in light forest fuels. Journal of Agricultural Research, 72(3), 93-121

Fried JS, Gilless JK, Spero J (2006). Analysing initial attack on wildland fires using stochastic simulation. International Journal of Wildland Fire, 15(1), 137-146

Friedman J, Hastie T, Tibshirani, R (2001). The elements of statistical learning (Vol. 1). Springer, Berlin: Springer series in statistics.

Gebert KM, Calkin DE, Yoder J (2007). Estimating suppression expenditures for individual large wildland fires. Western Journal of Applied Forestry, 22(3), 188-196

Geweke J, Tanizaki H (2001). Bayesian estimation of state-space models using the Metropolis–Hastings algorithm within Gibbs sampling. Computational Statistics & Data Analysis, 37(2), 151-170

Gunderson LH, Snyder JR (1994). Fire patterns in the southern Everglades. Everglades: The ecosystem and its restoration, 291-306

Hernandez C, Drobinski P, Turquety, S (2015, July). How much does weather control fire size and intensity in the Mediterranean region?. In Annales Geophysicae (Vol. 33, No. 7, pp. 931-939)[a]

Hernandez C, Keribin C, Drobinski P, Turquety S (2015). Statistical modelling of wildfire size and intensity: a step toward meteorological forecasting of summer extreme fire risk. In Annales Geophysicae (Vol. 33, No. 12, pp. 1495-1506)[b]

Hilbe JM (2011). Negative binomial regression. Cambridge University Press.

Johansen MP, Hakonson TE, Breshears DD (2001). Post□fire runoff and erosion from rainfall simulation: contrasting forests with shrublands and grasslands. Hydrological processes, 15(15), 2953-2965

Kasischke ES, Williams D, Barry D (2002) Analysis of the patterns of large fires in the boreal forest region of Alaska. International Journal of Wildland Fire, 11:131-144

Keeley JE, Safford H, Fotheringham CJ, Franklin J, Moritz M (2009). The 2007 southern California wildfires: lessons in complexity. Journal of Forestry, 107(6), 287-296

Khabarov N, Moltchanova E, Obersteiner M (2008). Valuing weather observation systems for forest fire management. IEEE Systems Journal, 2(3), 349-357

Kolden CA, Lutz JA, Key CH, Kane JT, van Wagtendonk JW (2012). Mapped versus actual burned area within wildfire perimeters: characterizing the unburned. Forest Ecology and Management, 286, 38-47

Koniak S (1985). Succession in pinyon-juniper woodlands following wildfire in the Great Basin. The Great Basin Naturalist, 556-566

Kot M (2001). Elements of mathematical ecology. Cambridge University Press.

McKenzie D, O'Neill, SM, Larkin NK, Norheim RA (2006). Integrating models to predict regional haze from wildland fire. ecological modelling, 199(3), 278-288

Minnich RA, Bahre CJ (1995). Wildland fire and chaparral succession along the California Baja-California boundary. International Journal of Wildland Fire, 5(1), 13-24

Mirabelli MC, Künzli N, Avol E, Gilliland FD, Gauderman WJ, McConnell R, Peters JM (2009). Respiratory symptoms following wildfire smoke exposure: airway size as a susceptibility factor. Epidemiology (Cambridge, Mass.), 20(3), 451

Moeltner K, Kim MK, Zhu E, Yang W (2013). Wildfire smoke and health impacts: A closer look at fire attributes and their marginal effects. Journal of Environmental Economics and Management, 66(3), 476-496

Morton DC, Roessing ME, Camp AE, Tyrrell ML (2003). Assessing the environmental, social, and economic impacts of wildfire. GISF Research Paper, 1

Moritz MA, Parisien MA, Batllori E, Krawchuk MA, Van Dorn J, Ganz DJ, Hayhoe K (2012). Climate change and disruptions to global fire activity. Ecosphere, *3*(6), 1-22

Murray JD (2002). *Mathematical Biology I. An Introduction* (Vol. 17). New York: Springer.

Nelle PJ, Reese KP, Connelly JW (2000). Long-term effects of fire on sage grouse habitat. Journal of Range Management, 586-591

Petris G, Petrone S (2011). State space models in R. Journal of Statistical Software, 41(4), 1-25

Plummer M (2003, March). JAGS: A program for analysis of Bayesian graphical models using Gibbs sampling. In Proceedings of the 3rd international workshop on distributed statistical computing (Vol. 124, p. 125)

Schoenberg FP, Peng R, Woods J (2003). On the distribution of wildfire sizes. Environmetrics, 14(6), 583-592

Scott JH, Thompson MP (2014, May). Emerging concepts in wildfire risk assessment and management. In theLarge wildland fires conference

Taylor DF, Williams DT (1968). Severe storm features of a wildfire. Agricultural Meteorology, 5(5), 311-318

Taylor SW, Woolford DG, Dean CB, Martell DL (2013). Wildfire prediction to inform fire management: statistical science challenges. Statistical Science, 28(4), 586-615.

Thompson MP (2013) Modeling Wildfire Incident Complexity Dynamics. PLoS ONE 8: e63297

Turetsky MR, Amiro BD, Bosch E, Bhatti JS (2004). Historical burn area in western Canadian peatlands and its relationship to fire weather indices. Global Biogeochemical Cycles, 18(4)

van der Werf GR, Randerson JT, Giglio L, Collatz GJ, Kasibhatla PS, Arellano AF (2006). Interannual variability in global biomass burning emissions from 1997 to 2004. Atmospheric Chemistry and Physics, 6(11), 3423-3441

Van Wagner CE (1969). A simple fire-growth model

Van Wagtendonk JW, Lutz JA (2007). Fire regime attributes of wildland fires in Yosemite National Park, USA. Fire Ecology, 3(2), 34-52

Veraverbeke S, Sedano F, Hook SJ, Randerson JT, Jin Y, Rogers BM (2014) Mapping the daily progression of large wildland fires using MODIS active fire data. International Journal of Wildland Fire, 23:655-667

Winsor CP (1932). The Gompertz curve as a growth curve. Proceedings of the national academy of sciences, 18(1), 1-8

Yildirim I (2012). Bayesian Inference: Gibbs Sampling. Technical Note, University of Rochester

Zhang, X., Kondragunta, S., & Quayle, B. (2011). Estimation of biomass burned areas using multiple-satellite-observed active fires. IEEE Transactions on Geoscience and Remote Sensing, *49*(11), 4469-4482

Chapter 2. ENVIRONMENTAL AND LANDSCAPE PREDICTORS OF WILDFIRE GROWTH AND FINAL SIZE ACROSS ECOREGIONS OF THE CONTERMINOUS USA

2.1 INTRODUCTION

Predictive models of wildfire activity are profoundly valuable to fire managers in the planning of effective suppression operations and assisting with decision-making at broad geographic scales. Predictive models of wildfire activity are also useful to researchers, who oftentimes want to predict wildfire behavior under hypothetical environmental conditions such as past and future climates. Wildfire prediction systems can range in complexity from spatially explicit physically based simulations (Williams et al. 2014) to regression models (Cortex and Morais 2007). The end goal is usually the same regardless, input environmental data and output predictions of wildfire activity.

There are a number of challenges to constructing predictive wildfire activity systems, one of which is the ambiguity in defining wildfire activity. Wildfire behavior is complex and can be quantified using multiple measurements including final size (Slocum 2010, Cardil et al. 2014, Turetsky et al. 2004, Butry et al. 2008, Martell and Sun 2008), duration (Westerling 2006), rate-of-spread (Werth and Ocha 1993, Cheney et al. 2012, Cruz et al. 2013) and daily area burned (Price et al. 2014, Billmire et al. 2014, Sedano and Randerson 2013). The growth measurements are used as proxies of overall fire severity and are frequently correlated, e.g. larger fires should be longer in duration. On the other hand, the measurements also describe unique characteristics of the wildfire's behavior and may be of particular importance to a specific application. Burn area measures are can be used by public health officials to quantify smoke exposure (Moeltner et

al. 2013) and carbon emissions (Van der Werf et al. 2006), duration measurements could be used to estimate suppression costs (Gebert et al. 2007), and growth rate measurements inform strategies and policies of firefighting professionals (Alexander and Thomas 2003).

Multiple measures of wildfire activity should be used whenever possible since univariate descriptions can lead to misleading assessments of fire severity. For example, ranking Florida fires by three different wildfire activity definitions corresponds to three unique conclusions about which fire was the most severe. If wildfire activity of fires is evaluated using final burn area, then the Bugaboo fire designated the most severe (MTBS 2017). If by rate-of-spread or duration, then the Big Scrub and Honey prairie would be respectively classified as the most severe (Cooper 1970, Inciweb 2017). Hence, to better describe the complexity of wildfire activity and its relationship to the environment, it is prudent to look at a variety of characteristics.

In addition to the ambiguity of defining wildfire activity, constructing predictive models can be challenging since the process is controlled by spatially varying environmental relationships and the same suite of environmental changes could have the opposite effect on fire behavior depending on where the fire is burning. For example, in fuel-limited ecosystems like deserts and grasslands, fire activity should be elevated when dry years follow extended periods of above-average precipitation. In these ecosystems, flammable biomass is often dry due to the long-term climate, but without adequate precipitation, insufficient in quantity to carry large fires. In contrast, climate-limited ecosystems like temperate forests have abundant biomass but require a sufficiently dry environment to cure the fuels (Meyn et al. 2007, Krawchuck et al. 2011, Barbero et al. 2014). Spatial variability in relationships between wildfire activity and the environment has been observed in multiple regions and growth measurements. Climate has been observed to disproportionately influence the probability of wildfire occurrence across ecosystems

within the continental United States (Hawbaker et al. 2013), and the correlation of Palmer Drought Severity Index and fire season severity dramatically changes across the Western United States (Westerling et al. 2003). High spatial variability in the best predictors of fire activity has also been observed in the Austrian Alps (Arpaci et al. 2013). Hence, to identify which environmental variables are important to wildfire behaviors; predictive models of wildfire activity should be regionally specific.

In this chapter, the relationship between wildfire activity and the environment will be quantified using a regionally specific multi-dimensional predictive model of wildfire activity in the Continental United States. This will be accomplished by decomposing cumulative burn area time series into six measurements of wildfire activity. The measurements will be calculated from written fire reports, and related to environmental variables using generalized linear models. The best model is selected using validation techniques, which identify the set of covariates with the lowest expected prediction error for a given location and behavior. The seasonality of wildfire activity is described by applying the models to historical climate data. In section 2.1 and 2.2, I describe how to decompose daily burn area time series into meaningful measurements and calculate them from burn area reports. Subsection 2.3 describes the environmental covariates that will be used in the predictive models. Subsection 2.4 describes the generalized linear model formulation for each growth measurement, as well as a method of describing dependence between growth measurements. The model selection and validation methods are described in subsection 2.5 and the application to historical weather data in subsection 2.6. In section 3, I discuss the results and summarize the effect of each covariate on wildfire behaviors in subsection 3.1, and analyze predicted intra-annual trends in wildfire behavior in subsection 3.2. I will close this paper in Section 4 with a discussion of the results, their implications and context within

current research.

2.2 METHODS

2.2.1 *Describing fire progression using growth measurements*

The sizes of individual wildfires are typically reported at a daily time step and can be approximated using an S-shaped curve (Figure 2.1a). From these curves, a set of four growth characteristics can be calculated that describe important aspects of a fire's growth. These four growth characteristics will be referred to as the final burn area (k), peak growth (m), lag period (l) and containment period (c). The final burn area represents the total amount of burn area once the fire has stopped all growth. The peak growth represents the percentage of the final area that burned during the day with the largest change in size. The lag period is the number of days from ignition until peak growth and the containment period is how long it takes after peak growth for the fire to be put out (Figure 2.1b). Lag period zero corresponds to the largest change in size occurring immediately upon ignition, that is on day zero. Containment period zero corresponds to immediate containment following the largest daily increment. Each of these growth characteristics measures a unique aspect of the wildfire growth curve. Final burn area is a measure of the incident size, while the other three variables being related to duration. The duration of the time series is $D = l + c + 1$ and $D \geq \lceil 1/m \rceil$.

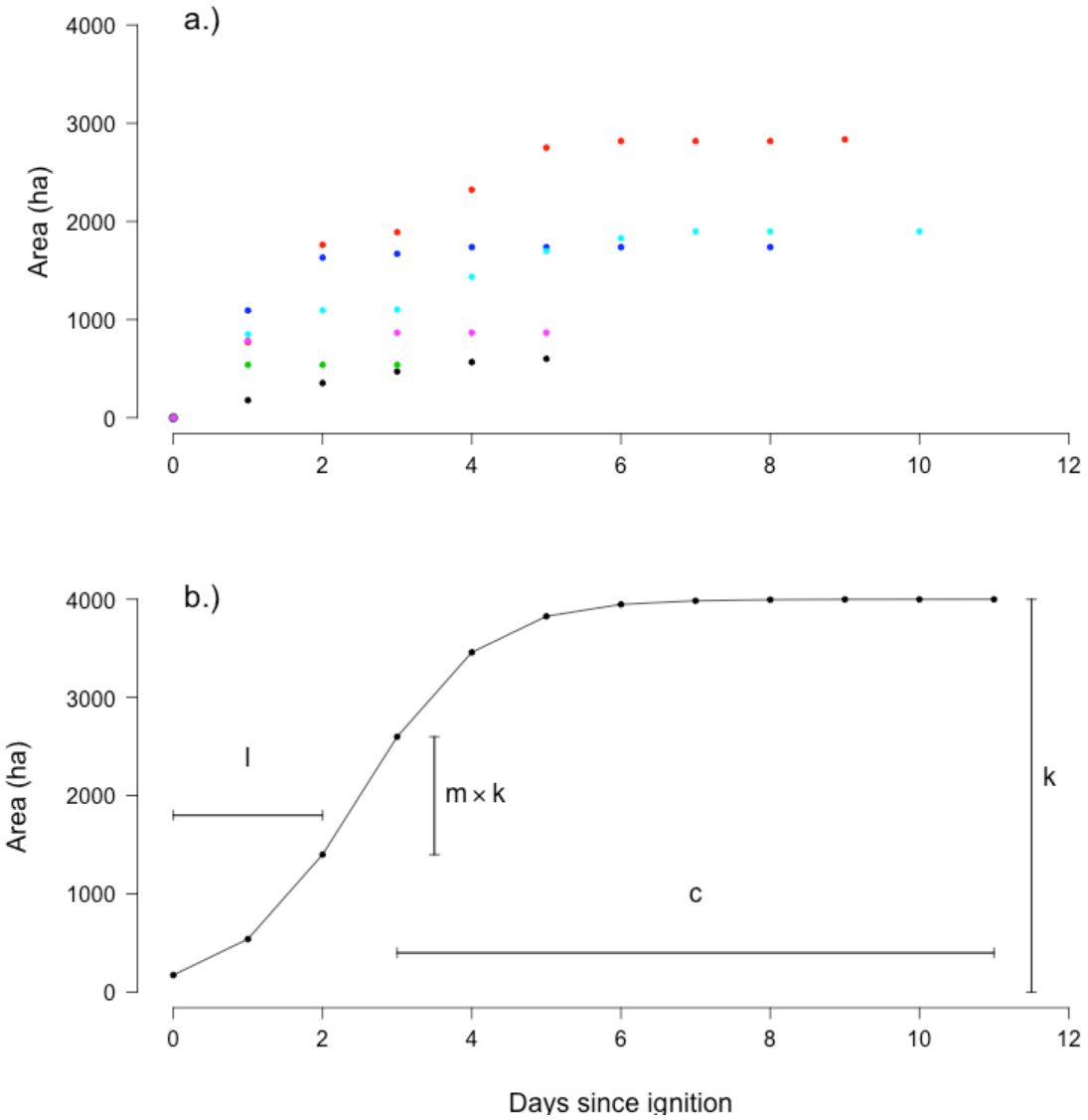

Figure 2.1 Observed growth characteristics for six wildfires (a). Example growth curve illustrating each of the growth characteristics (b). In (b), k represents the final area burned by the fire, m is the percentage of the final burn area that was consumed during the largest daily area burned, l is the number of days between the ignition and the largest daily run and c is the number of days between the largest daily area burned and the last day of the fire.

2.2.2 *Incident report processing*

I compiled a dataset of the four growth characteristics for 2,013 large fire incidents from the National Fire and Aviation Management Website (FAMWEB; https://fam.nwcg.gov/fam-web/hist_209/report_list_209, accessed August 2015). The website archives Incident Status Summary (ICS-209) reports for significant natural disasters throughout the United States. Reports were used to get estimates of the cumulative burn area time series and other information such as the incident name, coordinates and month of ignition. The final dataset of 2,013 events was a subset of the entire set of reports contained within the website. The final dataset included all events that labeled as "Wildland fire" or "Fire", within the Continental United States, and larger than 404 hectares. Some events were removed because missing data made it impossible to calculate peak growth and lag period, or to prevent inclusion of incidents that may not have been extinguished during the reporting period. Specifically, fires whose maximum "% Contained" attribute never exceeded 90 percent were removed from the dataset. A total of 291 events were removed to reduce the inclusion of still burning fires, representing about 11 percent of the total large wildfire incidents.

Each size time series was cleaned to correct any recorded decreases in fire size, which often occurred when better mapping technology became available during an incident. Cleaning was performed by iteratively comparing the future burn area measurement with the previous. If the previous day's measurement was larger than the future measurement, it was replaced with the future one. When multiple values existed on the same day only the largest record was retained.

The four growth characteristics; the final burn area (k), peak growth (m), lag period (l) and containment period (c), were calculated from the cleaned time series. The final burn area

was set equal to the "Size/Area involved" attribute from the final incident report; presumably the most reliable estimate of final burn area from the entire collection of records. Days until containment defined by subtracting the lag period from fire duration minus one; duration is the number of days from the reported ignition date until final report date. Peak growth may correspond to multiple days of the fire, so lag period was defined as the first daily change in burn area that is equal to peak growth. The final burn area data was transformed via $Z = \ln(\frac{k}{404})$. Logging reduced the influence of very-large fires and thresholding the data moved the empirical distribution so $Z > 0$. Attempts to model the untransformed data failed to yield regional models that included any covariates. Increases in wildfire activity were expected to correspond to an increase in final burn area, lag periods and containment periods, as well as decrease peak growth (Figure 2.2).

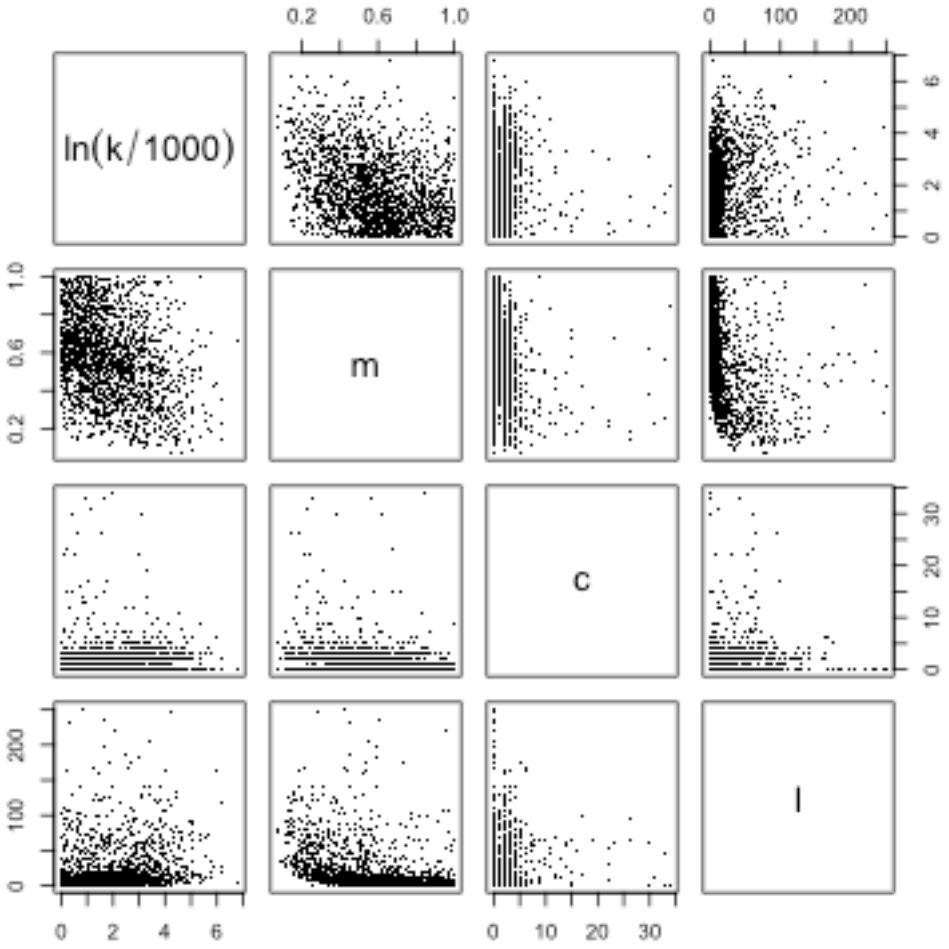

Figure 2.2 Scatterplot matrix of each of the 2,013 growth characteristics as calculated from the ICS-209 reports.

2.2.3 *Ecosystem assignment and covariates*

Using the incident coordinates from the final ICS-209 report, each event was assigned to one of eight ecosystems (Figure 2.3). The ecosystem definitions were built from the "Major Habitat Type" attribute in a spatial dataset developed by the Nature Conservancy and the World Wildlife Fund (Olson, D. M. and E. Dinerstein, 2002) and are broadly similar physiographic regions in terms of climate and vegetation structure. "Temperate Conifer Forests" were further split between Eastern (East of 101°) and Western United States. Because ICS-209 data is not spatially explicit, it cannot be know for certain whether any of the incidents crossed an ecosystem boundary during the fires lifetime. The majority of incidents in each group burned well within the interior of the ecosystem boundaries and will tend to be separated by topographic features.

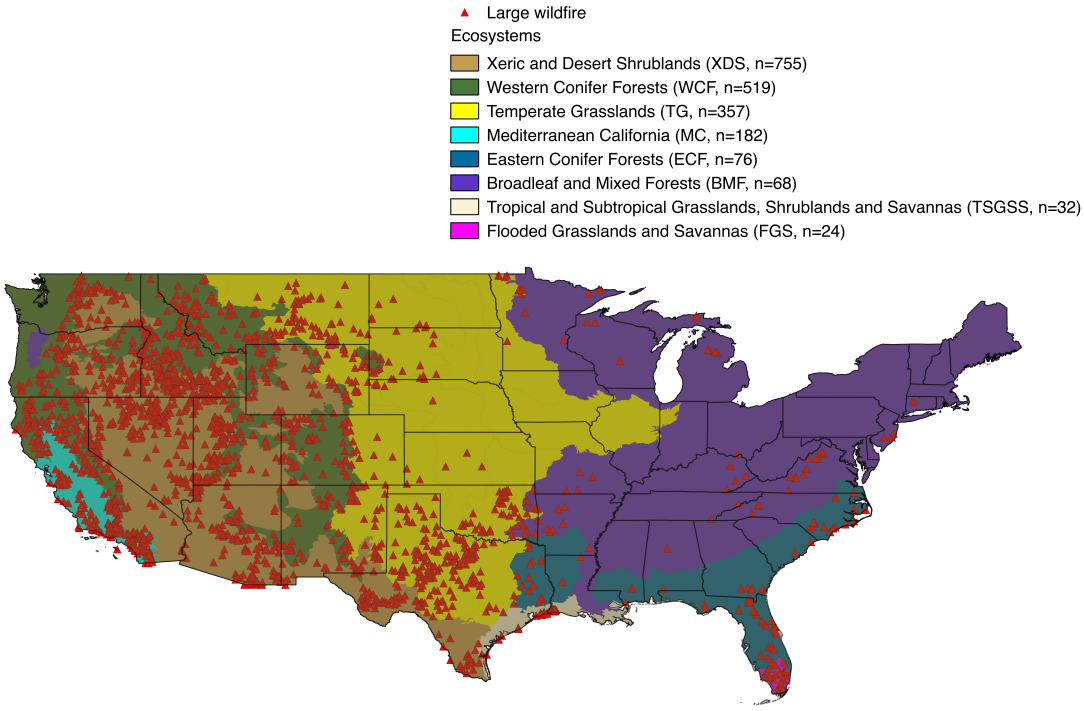

Figure 2.3 Map of incident locations and ecosystem boundaries for 2,013 incidents in final dataset. The number of wildfires in each ecoregion in parenthesis.

Table 2.1 Meteorological, anthropogenic and topographic variables.

Variable	Source	Units
Wind speed at 10m	Abatzoglou 2012	Meters/second
Specific humidity	Abatzoglou 2012	Percent
Precipitation total	Abatzoglou 2012	Millimeters
Temperature anomaly	Abatzoglou 2012	Score
Human land use	NLCD 2015	Percent
Elevation	Abatzoglou 2012	Meters
Latitude	Abatzoglou 2012	Degrees North

Time and location of each incident were combined with spatially explicit data describing potential predictors of wildfire growth (Table 2.1). Meteorological variables were based on monthly averages of daily gridded metrological data on a $1/24^{th}$ degree spatial grid (Abatzoglou 2012). Meteorological variables included wind speed, specific humidity, precipitation totals over the last 3, 6, 12 and 24 months, and three Min/Max mean temperature (Weiss et al. 2005) anomalies. Seasonality is a temperature anomaly referenced by all monthly temperatures at a given location. The 1-month temperature anomaly is an anomaly referenced by temperatures specific to each month. The 12-month temperature anomaly is an anomaly referenced by rolling 12-month averages of temperature values specific to each month. All reference periods were computed with data from 1979-2001. In addition to meteorological variables, three landscape variables, the latitude, elevation and percent human land use, were also included. To calculate percent human land use, land cover data from the 2011 National Land Cover Database was reclassified into "human influence" and "non-human influence" categories, where the former included developed and planted/cultivated land classes and the latter included barren, forest, shrubland and wetlands classes. The open water class was ignored (Homer 2015).

2.2.4 *Generalized linear models*

A series of generalized linear models (Faraway 2006) were built to describe regional influences of the predictor variables on each of the six growth characteristics. Visual inspection of marginal QQ-plots suggested that the chosen probability distribution of each response adequately described the four growth characteristics (Appendix A). Final burn area (transformed via $z = \ln(\frac{X}{404})$) was fit using a gamma response with log link. The gamma response of final burn area was appropriate given the likely appearance of power-law behavior (Alvarado et al. 1998, Slocum 2010), which would be gamma distributed after the logging and thresholding

(Dallas 1976). The log-link guarantees that the expected response is greater than zero, which is consistent with the quantities the four growth characteristics are measuring, and assumes that the effects of the predictors are multiplicative on the mean. Peak growth was fit using a beta response with logit link. Count data used a negative binomial response with log link.

To account for potential dependence between the growth characteristics, I also constructed two separate models that predicted two wildfire activity indexes. The indexes were calculated as the first principle component of three values: ln (D), $-\ln(m)$ and ln $(\frac{k}{404})$, using either the total and regional subsets of the dataset. The regional wildfire activity index (RWAI) was calculated using the data specific to the target region and the global wildfire activity index (GWAI) was calculated using all 2,013 fires. Wildfire activity index models had an identify link and Gaussian response. In total, there were six growth characteristic models for each region; four were directly calculated from the burn area time series and two aggregate wildfire activity indexes.

2.2.5 *Model selection and validation*

The three-split holdout method was used for model selection and test error estimation (Dua and Chowriappa 2012). Events were assigned into one of three mutually independent groups that are classified as the training, selection and validation datasets. The training dataset contained fires from years 2002, 2003, 2005, 2006, 2009 and 2012 and was used to create the initial set of models for each growth characteristic and each region. The large initial set of models contained all linear combinations of the covariates constrained such that at most one precipitation total variable (either 3,6,12 and 24-month) was included. The selection dataset contained fires from the years 2008 and 2011. From the large initial set of models, the model that minimized the mean squared prediction error on the selection dataset was chosen. The validation

dataset contained fires from the years 2004, 2007 and 2013, and was used to test the predictive ability of the models on independent data. Validation was assessed in two ways. First, a simple least squares model was fit to the observed error vs. predictions using observations from the validation dataset. Perfect prediction of the observations would imply that the errors and predictions fell on the horizontal line, $y = 0$. If an alternative linear model better described the scatter, then the model was classified as miscalibrated, otherwise it was classified as well calibrated. A likelihood ratio test with 10 percent rejection rate assessed the joint significance. The validation dataset was also used to calculate the predicted residual error sum of squares (PRESS) statistic for each model.

2.2.6 *Application to historical data*

The set of 48 (6 growth characteristics × 8 regions) best models were applied to daily gridded historical climate data from 1979-2015 (Abatzoglou 2012) to create monthly maps of predicted growth characteristics values from 1981-2015. For each of the eight regions, monthly time series of each of the growth characteristics was taken from 100 random pixels. Seasonal changes in the growth characteristics at the sampled locations were assessed graphically with boxplots.

2.3 RESULTS

2.3.1 *Model summary*

The relationship between the environment and wildfire activity could drastically change depending on the region and growth characteristic. Regional differences were very common and the same growth characteristic may either have a negative, positive or no relationship with a given predictor depending on the location. Differences could also be seen across growth

characteristics within the same region, often with peak growth and lag period disagreeing with the remaining growth characteristics. All ecosystems but the Eastern Conifer Forests (ECF) had at least one covariate that had both negative and positive associations with wildfire activity as measured by the six growth characteristics. Covariates where disagreements across growth characteristics were commonly observed include specific humidity, 1-month temperature anomalies, 12-month temperature anomalies and wind speed covariates.

For western regions, the Western Conifer Forests (WCF), Xeric and Desert Shrublands (XDS), Temperate Grasslands (TG) and Mediterranean California (MC), increasing wind speed were usually predicted to increase wildfire activity. The reverse relationship was predicted in the Eastern regions such as the Broadleaf and Mixed Forests (BMF), ECF, Tropical and Subtropical Grasslands, Shrublands and Savannas (TSGSS) and Flooded Grasslands and Shrublands (FGS), where increasing wind speeds often decreased wildfire activity. However, exceptions to this exist in both the Eastern and Western regional blocks.

Increases in specific humidity tended to decrease wildfire activity, with half of the regions predicting only negative relationships. Two western regions, WCF and MC, reported a positive association between specific humidity and lag period. In contrast, increases in specific humidity tended to increase wildfire activity in ECF and BMF. Increasing specific humidity nearly always reduced final burn area and to a lesser extent, the wildfire activity indexes.

Increased human land use was usually predicted to reduce wildfire activity. In most of the Western block, human land use was predicted to have a negative effect on wildfire activity, as was seen in WCF, XDS and TG. MC growth characteristic models were an exception and predicted that increased human land use tended to increase wildfire activity. Human land use was less often included in growth characteristic models in the Eastern block, and was never used in

the ECF.

Elevation was used most often used with the lag period growth characteristic. Increased elevation was nearly always associated with a predicted increase in the lag period, although the reverse was observed in FGS. With the exception of lag period, elevation was included as a covariate relatively infrequently, and had a mixed effect of wildfire activity. Increased elevation was predicted to decrease peak growth in MC and BMF, but increased it in XDS, ECF and FGS.

Latitude had a variable of effect on wildfire activity depending on the region and growth characteristic, and was seldom used in most of the regions. TSGSS and FGS were notable exceptions, in both regions nearly all growth characteristic model included latitude, with a positive effect on wildfire activity in TSGSS and negative effect in FGS. Both regions were relatively small compared to the other six regions.

When included, seasonality tended to have an overall positive influence on wildfire activity. Seven of the eight regions predicted only positive relationships between seasonality and wildfire activity, and only in FGS was the reverse observed. While the WCF models included seasonality in all six growth characteristic models, most regions included it for less than half.

1-month temperature anomalies were often used to predict peak growth, although their effect was regionally variable. In WCF, TG and FGS, above-average monthly temperatures were associated with increases in peak growth, and the reverse was observed in XDS, MC and TSGSS. In BMF, 1-month temperature anomalies were included in all growth characteristic models except for peak growth and always increased wildfire activity. Otherwise, the relationship between this covariate and wildfire activity was highly variable across regions and growth characteristics.

Like 1-month temperature anomalies, the effect of 12-month temperature anomalies on

wildfire activity was highly variable across regions and growth characteristics. 12-month temperature anomalies were mostly used in WCF, and to a lesser extent in XDS and FGS. For most other regions, 12-month temperature anomalies were seldom included and were never used in any BMF models.

The effect of precipitation totals on the growth attributes was variable, both in terms of the number of months used to calculate the total, as well as the sign of the effect. 12-month and 24-month precipitation totals seemed to be favored in MC and TSGSS. Sub-annual precipitation total were favored in WCF, TG and BMF. In eastern regions, increased precipitation was generally predicted to decrease wildfire activity, while the reverse was more common in western regions.

The models for RWAI and GWAI were usually near identical. Only in BMF, was there a difference between the suite of variables included in the RWAI and GWAI models; the GWAI model omitted specific humidity. The best set of predictors in the wildfire activity models often reflected the consensus among other four models in that region (Figure 2.4).

The PRESS statistic varied greatly between region and growth characteristic (Table 2.2). Peak growth was best predicted in TSGSS and was worst in FGS. Final burn area was best predicted in BMF and worst in ECF. Lag period was best predicted in MC and was worst predicted in ECF. Containment period was best predicted in TSGSS and was least predictable in ECF. Lag period models tended to have a lower prediction error than containment period models. ECF models tended to do have very high PRESS values to other regions.

There was no evidence of miscalibration for any models in XDS or WCF. In FGS, there was no detectable miscalibration in any models, with the exception of the burn area models. Only the peak growth model and global wildfire activity index was well calibrated in TG. Peak

growth, final burn area and lag period models were miscalibrated in MC. The wildfire activity indexes showed detectable miscalibration in ECF, as did lag period and containment period in BMF. In total, 12 of the 48 growth characteristic models had detectable miscalibration when assessed using the validation data.

Figure 2.4 The region specific relationships between each growth characteristic and covariate. Each character corresponds to a growth characteristic and the color the effect. Red denotes an increase and blue, a decrease in wildfire activity as measured by corresponding growth characteristic. Note that a decrease in peak growth (m) is associated with increased wildfire activity, while the reverse is true for the global wildfire activity index (g), regional wildfire activity index (r), final burn area (k), lag period (l) and containment period (c).

Table 2.2 Square root PRESS statistic and rank for each ecoregion and growth measure.

	ECF	WCF	BMF	TSGSS	TG	FGS	MC	XDS
m	0.482	0.463	0.415	0.368	0.41	0.573	0.439	0.431
	(7)	(6)	(3)	(1)	(2)	(8)	(5)	(4)
k	1.257	1.135	0.911	0.925	0.958	1.034	1.173	1.106
	(8)	(6)	(1)	(2)	(3)	(4)	(7)	(5)
l	2.095	1.956	1.163	1.361	1.24	1.799	0.84	1.687
	(8)	(7)	(2)	(4)	(3)	(6)	(1)	(5)
c	8.063	5.962	2.872	2.213	2.474	3.274	5.559	3.767
	(8)	(7)	(3)	(1)	(2)	(4)	(6)	(5)
RWAI	1.335	1.204	0.967	1.046	0.914	1.173	1.026	1.049
	(8)	(7)	(2)	(4)	(1)	(6)	(3)	(5)
GWAI	1.36	1.166	1.065	1.187	1.073	1.256	1.052	1.135
	(8)	(5)	(2)	(6)	(3)	(7)	(1)	(4)

2.3.2 *Application to historical data*

Seasonal trends in wildfire activity varied between regions and by growth characteristic. In the WCF, wildfire activity indexes, burn area, lag period and containment period were maximized, and peak growth minimized, during the summer months. In XDS, burn area and lag period was predicted to be fairly constant throughout the year and both indexes were minimized in the summer months. TG summers tended to have smaller burn area and peak growth, as well as larger lag period and containment period growth characteristics. Both wildfire activity indexes were predicted to be fairly constant throughout the year. In MC, burn area, containment periods and peak growth were minimized, and the wildfire activity indexes were maximized in the summer months. The MC model of lag period showed no clear seasonal trend. BMF showed little seasonal trend in terms of burn area, lag period, containment and GWAI, although peak-growth was minimized and RWAI was maximized in the summer months. ECF burn area, containment period and wildfire activity indexes were maximized in the summer, while lag period was maximized in the late-spring/early-summer months. ECF peak growth models showed no clear seasonal trend. There was no clear trend in the TSGSS, other than a slight preference for long containment periods in the winter months. In FGS, burn area, containment periods and wildfire activity indexes were maximized and peak growth minimized in the winter months, while lag period showed no trend. A large proportion of the models had predicted trends in wildfire activity from 1981-2015 that approximately matched the observations from 2002-2013.

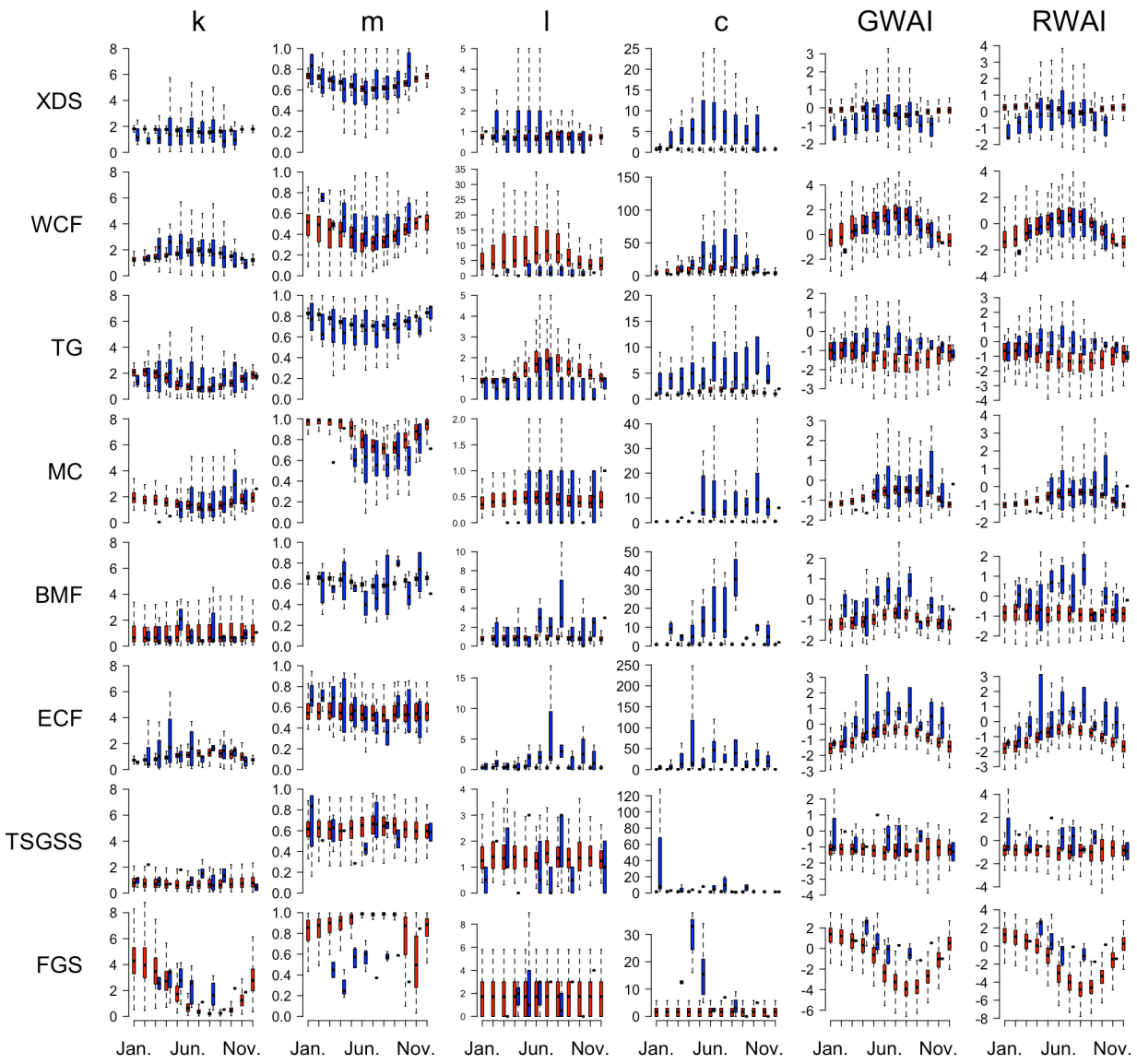

Figure 2.5 Boxplots of each of the predicted growth attributes from 100 random locations within each region from 1981-2015 by month; outliers have been removed. Observed growth parameter values from 2002-2013 are shown in blue and predictions are red. Outliers were not plotted to improve the visibility of seasonal trends.

2.4 DISCUSSION

Wildfire activity is complex process that can be described using multiple growth measurements and has many spatially varying influences including weather, fuel availability and topography. Constructing predictive models of wildfire activity will require approximating the complexity of the process and its relationship to the environment, which was done using a variety of strategies. Multi-dimensional aspects of wildfire activity were captured using multiple measurements. The effects of the environment on wildfire activity were accounted for by including important covariates and spatially variable trends were acknowledged by stratifying the data into biogeographically similar groups prior to fitting the generalized linear models. The strategies outlined in this chapter resulted in models that adequately predicted wildfire activity for the majority of ecosystems and growth characteristics.

2.4.1 *Complexity of wildfire activity*

The best predictors of wildfire activity often changed dramatically across regions or growth characteristics. Changes could be in the form of removal or addition of particular covariates, alterations of covariate effects, and changes in predictive ability. Even in nearby regions, spatial variability in the model complexity may be high. For instance, in FGS, lag period was best predicted using only landscape predictors, resulting in time-invariant predictions. In contrast, the geographically adjacent ECF model of lag period only included environmental variables and predicted changes over the year. Regionally specific relationships were common, as illustrated by the relationship between specific humidity and burn area in ECF and FGS. In ECF, increased specific humidity tended to increase final burn area, but the effect on final burn area was opposite in nearby FGS. Drastic regional variability in the predictability of certain growth characteristics was also observed. Final burn area was most predictable in the BMF

model, but the nearby ECF model was the least predictive final burn area model.

Model changes across growth characteristics within the same region were common. In the WCF, the effect of specific humidity and 12-month temperature anomalies on lag period was predicted to be opposite of the other growth characteristics in the region. It was nearly always lag period and peak growth that disagreed with the remainder of growth characteristics in a given region, which may suggest that the drivers of both growth characteristics are not closely related with the others (i.e. final burn area, containment period and the wildfire activity indexes). Meaningful comparisons between growth characteristics in the same region can only be done for lag period and containment period, since they are both measuring durations of certain wildfire events, and in every region, lag period had a lower prediction error than the containment period.

The complexity of wildfire activity and its relationship to the environment suggest that modeling multiple-dimensions of wildfire activity has a variety of benefits. Firstly, it better describes the details of wildfire activity that can otherwise be masked, as was seen in the Florida wildfires example. Secondly, it allows a method of measuring the strength of particular covariate on wildfire activity broadly. If only one of the growth characteristic models in the suite include a specific covariate, then it suggests that it might not be a broadly important driver of wildfire activity. In contrast, if all the models in the suite were in consensus about the effect of a particular covariate that might suggest that it was very important in that region. Third, by using multiple measures of wildfire activity it allows the models to be used in a broad variety of applications that sometimes require specific growth measurements.

2.4.2 *Regional-level models of growth characteristics*

Xeric and Desert Shrublands are an unambiguously fuel-limited ecosystems and as such, increases in wildfire activity would be predicted when drought activity follows above-average

precipitation levels. Lag period, containment period and the wildfire activity indexes were both positively associated with 12- and 24-month precipitation totals, which conforms to theoretical expectations. On the other hand, sub annual precipitation totals were negatively associated with final burn area and peak growth. The sub annual precipitation total variables are likely capturing seasonal trends in the growth characteristics and are likely be minimized in late summer. Specific humidity seemed to be a particularly important covariate in Xeric and Desert Shrublands, being included in all but the lag period model. Predictions of wildfire activity appear to be maximized during the summer and spring months, which is consistent with reports of peak fire season (Littell et al. 2009, Pyne 1982, Barbero et al. 2014). The models matched the seasonality of the observations reasonably well and generalized well to independent observations.

Western Conifer Forests would likely be categorized as a climate-limited ecosystem, as flammable biomass is abundant, but is dry less frequently than in Xeric and Desert and Shrublands. Wildfire activity should then be increased during periods of extended drought (Kulakowski 2011, Barbero et al. 2014). The consensus among the models was that 6-month precipitation totals were positively associated with wildfire activity, which did not conform to prior expectations. The seasonal fluctuations of the 6-month precipitation totals suggest that wildfire activity will tend to be minimized just before the onset winter precipitation and maximized in the beginning of the fire season. The consensus of models also predicted a positive effect of seasonality. The net effect is that wildfire activity is increased during the hottest months of the year, and fires that occur early in the wildfire season will be worse. Other important covariates included in most of the growth characteristic models were wind speed, human land use, and 12-month temperature anomalies. Predictions of wildfire activity seem to largely match

other research (Westerling et al. 2006, Barbero et al. 2014, Littell et al. 2009) and generalized well to independent observations.

Temperate grasslands are dominated by mostly herbaceous cover, which suggests that fuel availability may largely limit wildfire activity. Only peak growth was predicted to worsen (increase duration) wildfire activity when 24-month precipitation totals are increased. Final burn area and the wildfire activity indexes were negatively associated with 6-month precipitation totals, and lag period positively associated with 3-month precipitation totals. Other important variables were specific humidity and 1-month temperature anomalies. The reported effects of weather on wildfire activity is variable. Fire size has been negatively associated with humidity (Barbero et al. 2014, Reid et al. 2010), and precipitation, and positively associated with wind speed (Reid et al. 2010). The relative influence of weather covariates, like humidity, temperature and wind speed, can fluctuate over the year depending on soil moisture levels (Krueger et al. 2015). Peak fire season is challenging to define in the Temperate Grasslands since they occur nearly all year in across the region. In the Northern Great Plains, the summer-autumn months (Jun.-Sep.) are considered peak wildfire season (Littell et al. 2009), while fire occurrence and area burned in Oklahoma are highest during the non-summer months (Reid et al. 2010). Only the global wildfire activity index and peak growth were well calibrated, the fewest of any region.

Mediterranean California vegetation is a mix of woody and herbaceous cover, making prior predictions concerning the effect of precipitation somewhat difficult. The positive relationship with nearly all the growth characteristics and precipitation totals over long time scales suggest that the region is largely fuel-limited. One exception was observed in peak growth, which was negatively associated with 3-month precipitation totals. Specific humidity was another important covariate in Mediterranean California. Specific humidity was negatively

associated with wildfire activity indexes, final burn area and containment period, and positively associated with lag period. Humidity and temperature have been identified as important predictors of burn area in Southwestern and Central California (Yue et al. 2014). The peak fire season is variable within California, occurring anywhere early as April central California to winter (Nov.-Dec.) in Southern California (Westerling et al. 2004, Littell et al. 2009, Billmire et al. 2014). In Southern California, a significant contributor to wildfire activity are Santa Ana winds, which are seasonal wind patterns that typically occurring from September through April in Southern California. Final burn area and containment period seem to be elevated during winter months, perhaps corresponding to increases in in Santa Ana winds. In contrast, peak growth and wildfire activity indexes seemed to be worst during the summer months. Lag period did not show any strong seasonal trend. Given the importance of Santa Ana winds, it was surprising that wind speed was rarely included in the models.

Broadleaf and Mixed Forests have abundant fuel that is rarely dry, which suggests wildfire activity will be elevated during extended periods of drought (Barbero et al. 2014). While theoretically similar to Western Conifer Forests, the Broadleaf and Mixed Forests contains more hardwood species, which are less flammable (Harper et al. 2016). Unlike most of the regions, precipitation total variables were included relatively infrequently. When included, wildfire activity was best predicted by sub annual precipitation totals. Increases in 3-month precipitation were associated with increases in burn area and increases of 6-month precipitation reduced lag period and the wildfire activity indexes. In addition to sub seasonal precipitation totals, 1-month temperature anomalies are important to a number of growth characteristics. Peak wildfire activity occurs during the dormant season (Sept.-Apr.), when the canopy opened and leaf litter was dried from the increased sunlight exposure (Knapp et al. 2009). On the other hand, wildfire activity

seems to be at its highest in the summer-autumn months in the Great Lakes region (Barbero et al. 2014, Clark 1989). Most of the growth characteristics showed little seasonality with the exception of peak growth and RWAI, which predicted the worst activity during the summer months.

Eastern Conifer Forests vegetation structure is somewhat similar to that of Western Conifer Forests, but is a geographically distinct region. Like the Western Conifer Forests, wildfire activity was negatively associated with increased precipitation, however unlike Western Conifer Forests, the temporal scale of the precipitation total can drastically change between growth characteristics. Lag period and wildfire activity indexes are associated with sub seasonal precipitation totals. Burn area, peak growth and containment periods appear to be associated with 12- and 24-month precipitation totals, which is supported by research demonstrating precipitation increases lessens the likelihood of very-large fires (Barbero et al. 2014, Slocum et al. 2010). While the models tended to predict that the summer months were the worst time of year for wildfires, the reported fire season covers the first half of the year (Jan.-May) and is minimized during the warm/humid summer months (Slocum et al. 2010, Lafon 2010, Goodrick et al. 2009). The predictions reasonably matched the seasonal patterns of the observations.

Tropical and Subtropical Grasslands, Shrublands and Savannas are predominately herbaceous, like Temperate Grasslands, suggesting wildfire activity will be positively associated with increases in 12- and 24-month precipitation totals. Surprisingly, the reverse relationship was observed for all growth characteristics, with increased long-term precipitation levels predicted to reduce wildfire activity. Tropical and Subtropical Grasslands, Shrublands and Savannas have a long history of anthropogenic fire use, which may influence the observed trends in fire seasonality (Grace 2005), and like Temperate Grasslands, can burn during both the

growing and dormant season (Grace 1998). Prescribed burning is commonly performed during the winter (Hansmire et al. 1988). Latitude was a commonly used predictor in Tropical and Subtropical Grasslands, Shrublands and Savannas and most of the models predicted only minor seasonal changes. Tropical and Subtropical Grasslands, Shrublands and Savannas had only 32 wildfires in the growth characteristics dataset.

In Flooded Grasslands and Savannas, biomass is abundant and infrequently dry, suggesting that drought conditions should increase wildfire activity. Precipitation totals were used infrequently relative to other regions. When included, the wildfire activity indexes and final burn area were negatively associated with 3-month totals, and the peak growth worsened with increased annual precipitation levels. Wildfires in the Flooded Grasslands and Savannas have usually been predicted to be more severe in drought conditions (Slocum et al. 2010, Barbero et al. 2014). Like Tropical and Subtropical Grasslands, Shrublands and Savannas, latitude was a relatively important variable, with wildfire activity decreasing poleward in all growth characteristic models. With the exception of lag period, most definitions of wildfire activity are predicted to be at there most severe during the winter months. In South Florida fires, lightning ignitions typically occur during the summer-autumn (Jun.-Sep.) and human caused ignitions run in the winter-spring (Nov.-May), the latter season being typically associated with larger and longer fires (Slocum et al. 2010). Typically fires in the winter were human caused while those in the summer were lightning caused (Taylor 1981). Despite the small sample size, only the peak growth model had detectable miscalibration and with the exception of lag period, which used only landscape predictors, most of the models seem to conform to reports of wildfire activity seasonality. With only 24 wildfires, Flooded Grasslands and Savannas had the fewest observations to construct and validate the wildfire activity models.

2.4.3 *Limitations*

The predictive ability of the models differed by region, and errors could have been biased downward if there were few observations and a particularly predictable validation dataset. While the expected prediction error was minimized, caution should still be taken in interpreting the results from regions with limited data (i.e. FGS and TSGSS). Other combinations of predictors could have possibly achieved similar predictive performance and there were slight levels of model instability. Changes to the model selection algorithm, changes to the regional grouping of fires, and measurement errors, could change the best combination of predictors. This is important to note because multiple changes could be made in this analysis. Important predictors not measured in this analysis could be included such as topographic complexity (Holsinger et al. 2016), vegetation (Birch et al. 2015), wildfire suppression (Finney et al. 2009) and atmospheric stability (Werth et al. 2011). Moreover, model selection methods could be modified to allow multi-scalar influences of precipitation on predictive wildfire activity (Barbero et al. 2015). Either of those changes may alter the best combination of predictors and improve predictive performance. Application of this model to independent data will implicitly assume that environmental conditions will not be drastically different from those in the training data. For example, applying the models to future climate scenarios will assume that vegetation structure, fire suppression policies and human land use does not change. Covariate effects should always be interpreted within the context of the entire suite of variables in the model.

Limitations may also come from the limited quantity and quality of wildfire growth data. Daily reports of wildfire burn area are not compiled in all regions and consistent monitoring from satellite data has only available for a short time frame relative to climatological time scales (Taylor et al. 2013), and written reports are not always compiled for all incidents (Finney 2009).

Additional limitations come from trying to classify individual wildfire incidents, which can be somewhat ambiguous as multiple fires may be managed under a single name. Data quality of burn area time series can often be poor, which can make calculating the growth characteristics challenging. Burn area measurements often repeat the same burn area estimate many times during the last days of the CBA record, even after 100 percent containment, which can inflate containment period estimates. Given the limited resolution these measurements that burn area measurements are reported at, problems can arise from the burn area time series decomposition methods. For instance, the maximum percent daily burn and lag period sometimes occur on multiple days, which would not be well described by univariate measures. The temporal scale between the growth characteristics and the covariates could make interpretation of the environmental effects challenging. For instance, rapid growth of fire may be driven by sudden gusts of wind at short time scales, which would not necessarily be captured by monthly values.

Given the model uncertainty and data limitations, a comprehensive model sensitivity analysis should be performed to see how slight changes in the inputs and training data influence the model structure and output. Slight perturbations to the data could cause other models to be selected, dropping covariates from models can alter the estimates of the remaining ones and different GLM configurations could alter the selection of best predictors. This model instability may motivate the future use of multi-model predictions of wildfire activity (Arlot and Celisse 2010). Still, for many regions and covariates, the models predicted wildfire activity in a way that was consistent with independent observations, suggesting its has potential as a tool for researchers and fire mangers.

2.5 CONCLUSIONS

By looking at multiple growth characteristics, this analysis had provided a more complete

description of the wildfire's behavior than univariate approaches could and can be used in a number of applications in research and fire management. One particularly important application of the models would be in wildfire climatology. Models that well predicted important growth characteristics could be applied to climate change scenarios to predict future trends in wildfire activity. Similarly, historical weather data can be used to make predictions concerning wildfire activity in situations where wildfire growth data is unavailable. Another particularly valuable application of the models is the simulation wildfire burn area time series based on environmental data, which can be constructed from the growth characteristics using a variety of methods. One potential method could use the wildfire activity indexes to predict final burn area, peak growth, lag period, and containment period characteristics, better modeling the correlation between the growth characteristics. Another method could predict the final burn area, peak growth, lag period, and containment period characteristics independently from the appropriate models. Simulated fire scenarios could potentially be constructed using forecasted weather conditions, which can be used to assist with firefighting decisions at broader geographic scales. Models like FARSITE require wildfire duration as an input (Finney 2004), which can be informed from predictions from the wildfire activity index model, or the lag period and containment period models.

In addition to providing a collection of potentially useful wildfire activity models to researchers and fire managers, this analysis has also provided a general strategy for relating wildfire burn area time series to the environment, which can be used in future research that is interested in other environmental variables and regions. Fire managers and scientists may also benefit from the identification of regionally important predictors of wildfire activity and by describing the consensus of these relationships across growth characteristics, and these results

were particularly important in validating theoretical expectations concerning the effect of precipitation totals on wildfire activity (Krawchuck et al. 2011, Meyn et al. 2007).

In closing, the presented research has provided multiple tools and results that improve the understanding of complex relationships between the environment and wildfire activity. It may also serve to inform future quantitative analyses of wildfire growth and provide guidelines for relating burn area time series to the environment within a statistical framework that is easily accessible.

2.6 REFERENCES

Abatzoglou JT Development of gridded surface meteorological data for ecological applications and modellingi International Journal of Climatology. (2012)

Alexander ME, Thomas DA (2003) Wildland fire behavior case studies and analyses: Other examples, methods, reporting standards, and some practical advice. Fire Management Today, 63:4-12

Alvarado E, Sandberg,DV, Pickford SG (1998). Modeling large forest fires as extreme events. National Emergency Training Center

Arlot S, Celisse A (2010). A survey of cross-validation procedures for model selection. Statistics surveys, 4, 40-79

Arpaci A, Eastaugh CS, Vacik H (2013). Selecting the best performing fire weather indices for Austrian ecoregions. Theoretical and Applied Climatology, 114(3-4), 393-406

Barbero R, Abatzoglou JT, Steel EA, Larkin NK (2014). Modeling very large-fire occurrences over the continental United States from weather and climate forcing. Environmental research letters, 9(12), 124009

Barbero R, Abatzoglou JT, Kolden CA, Hegewisch KC, Larkin NK, Podschwit, H (2015). Multi scalar influence of weather and climate on very large fires in the Eastern United States. International Journal of Climatology, 35(8), 2180-2186

Billmire M, French NH, Loboda T, Owen RC, and Tyner M (2014). Santa Ana winds and predictors of fire progression in southern California. International Journal of Wildland Fire, 23.8, 1119-1129

Birch DS, Morgan P, Kolden CA, Abatzoglou JT, Dillon GK, Hudak AT, Smith A (2015). Vegetation, topography and daily weather influenced burn severity in central Idaho and

western Montana forests. Ecosphere, 6(1), 1-23

Bradstock RA, Hammill KA, Collins L, Price O (2010). Effects of weather, fuel and terrain on fire severity in topographically diverse landscapes of south-eastern Australia. Landscape Ecology, 25(4), 607-619

Butry DT, Gumpertz M, Genton MG (2008). The production of large and small wildfires. The Economics of Forest Disturbances: Wildfires, Storms, and Invasive Species, 79, 79

Cardil A, Eastaugh CS, Molina DM (2014). Extreme temperature conditions and wildland fires in Spain. Theoretical and Applied Climatology, 1-10

Cheney NP, Gould JS, McCaw WL, Anderson WR (2012). Predicting fire behaviour in dry eucalypt forest in southern Australia. Forest Ecology and Management, 280, 120-131.

Clark JS (1989). Effects of long-term water balances on fire regime, north-western Minnesota. The Journal of Ecology, 989-1004

Cortez P, Morais A (2007). "A Data Mining Approach to Predict Forest Fires using Meteorological Data." In MFS J Neves, J Machado (eds.), "New Trends in Artificial Intelli- gence," volume Proceedings of the 13th EPIA 2007, pp. 512–523. Portuguese Conference on Artificial Intelligence, Guimara˜es, Portugal. ISBN 13 978-989-95618-0-9

Cooper JW 1970. The big scrub fire. p. 1-2

Cruz, MG, Alexander ME Uncertainty associated with model predictions of surface and crown fire rates of spread. Environmental Modelling & Software 47 (2013): 16-28

Dallas AC (1976). Characterizing the Pareto and power distributions. Annals of the Institute of Statistical Mathematics, 28(1), 491-497

Dua S, Chowriappa P (2012). Data mining for bioinformatics. CRC Press.

FAMWEB; https://fam.nwcg.gov/fam-web/hist_209/report_list_209, accessed August

2015

Finney MA (2004). FARSITE: Fire area simulator: model development and evaluation. Ogden, UT: US Department of Agriculture, Forest Service, Rocky Mountain Research Station.

Finney MA, Grenfell IC, McHugh CW (2009). Modeling containment of large wildfires using generalized linear mixed-model analysis. Forest Science, 55(3), 249-255

Gebert KM, Calkin DE, Yoder J (2007). Estimating suppression expenditures for individual large wildland fires. Western Journal of Applied Forestry, 22(3), 188-196

Goodrick SL, Hanley, DE (2009). Florida wildfire activity and atmospheric teleconnections. International Journal of Wildland Fire, 18(4), 476-482

Grace JB (1998). Can prescribed fire save the endangered coastal prairie ecosystem from Chinese tallow invasion. Endangered Species Update, 15(5), 70-76

Grace JB, Allain LK, Baldwin HQ, Billock AG, Eddleman WR, Given AM,Moss R (2005). Effects of prescribed fire in the coastal prairies of Texas

Hansmire JA, Drawe DL, Wester DB, Britton CM (1988). Effect of winter burns on forbs and grasses of the Texas coastal prairie. The Southwestern Naturalist, 333-338

Hawbaker TJ, Radeloff VC, Stewart SI, Hammer RB, Keuler NS, Clayton MK (2013). Human and biophysical influences on fire occurrence in the United States. Ecological applications, 23(3), 565-582

Harper CA, Ford WM, Lashley MA, Moorman CE, Stambaugh MC (2016). Fire effects on wildlife in the Central Hardwoods and Appalachian regions, USA. Fire Ecology, 12(2), 127-159

Holsinger L, Parks SA, Miller C. Weather, fuels, and topography impede wildland fire spread in western US landscapes. Forest Ecology and Management 380 (2016): 59-69

Homer CG, Dewitz JA, Yang L, Jin S, Danielson P, Xian G, Coulston J, Herold ND, Wickham JD, Megown K (2015), Completion of the 2011 National Land Cover Database for the conterminous United States-Representing a decade of land cover change information. Photogrammetric Engineering and Remote Sensing, v. 81, no. 5, p. 345-354

InciWeb developed and maintained by USDA Forest Service, Fire and Aviation Management, helpdesk@dms.nwcg.gov. (n.d.). Retrieved March 09, 2017, from https://inciweb.nwcg.gov/incident/2214/

Krawchuk MA, Moritz MA Constraints on global fire activity vary across a resource gradient. Ecology 92.1 (2011): 121-132

Krueger ES, Ochsner TE, Engle DM, Carlson JD, Twidwell D, Fuhlendorf SD (2015). Soil moisture affects growing-season wildfire size in the Southern Great Plains. Soil Science Society of America Journal, *79*(6), 1567-1576

Kulakowski D, Jarvis D (2011). The influence of mountain pine beetle outbreaks and drought on severe wildfires in northwestern Colorado and southern Wyoming: a look at the past century. Forest Ecology and Management, 262(9), 1686-1696

Lafon CW (2010). Fire in the American South: vegetation impacts, history, and climatic relations. Geography Compass, 4(8), 919-944

Li Z, Nadon S, Cihlar J (2000) Satellite-based detection of Canadian boreal forest fires: Development and application of the algorithm. International Journal of Remote Sensing, 21:3057-3069

Littell JS, McKenzie D, Peterson DL, Westerling AL (2009). Climate and wildfire area burned in western US ecoprovinces, 1916–2003. Ecological Applications, 19(4), 1003-1021

Martell DL, Sun H (2008). The impact of fire suppression, vegetation, and weather on the

area burned by lightning-caused forest fires in Ontario. Canadian Journal of Forest Research, 38(6), 1547-1563

Meyn A, White PS, Buhk C, Jentsch A. (2007). Environmental drivers of large, infrequent fires: the emerging conceptual model. Progress in Physical Geography, 31(3), 287-312

Moeltner K, Kim MK, Zhu E, Yang W (2013). Wildfire smoke and health impacts: A closer look at fire attributes and their marginal effects. Journal of Environmental Economics and Management, 66(3), 476-496

MTBS. (n.d.). Retrieved March 09, 2017, from http://www.mtbs.gov/dataaccess.html

Nyman JA, Chabreck RH (1995). Fire in coastal marshes: history and recent concerns. In Fire in wetlands: a management perspective. Proceedings of the tall timbers fire ecology conference (Vol. 19)

Olson DM, Dinerstein E, Powell GV, Wikramanayake ED (2002). Conservation biology for the biodiversity crisis. Conservation Biology, 16(1), 1-3

Price OF, Borah, R, Maier SW (2014). Role of weather and fuel in stopping fire spread in tropical savannas. Austral Ecology, 39(2), 135-144

Pyne SJ(1982). Fire in America. A cultural history of wildland and rural fire. Princeton University Press.

Reid AM, Fuhlendorf SD, Weir JR (2010). Weather variables affecting Oklahoma wildfires. Rangeland ecology & management, 63(5), 599-603

Sedano F, Randerson JT (2014). Multi-scale influence of vapor pressure deficit on fire ignition and spread in boreal forest ecosystems. Biogeosciences, 11(14), 3739-3755

Slocum MG, Beckage B, Platt WJ, Orzell SL, Taylor W (2010). Effect of climate on fire

size: a cross-scale analysis. Ecosystems, 13(6), 828-840

Taylor, DL Fire history and fire records for Everglades National Park, 1948-1979 [Florida]. Report/South Florida Research Center (USA) (1981)

Turetsky MR, Amiro BD, Bosch E, Bhatti JS (2004). Historical burn area in western Canadian peatlands and its relationship to fire weather indices. Global Biogeochemical Cycles, 18(4)

van der Werf GR, Randerson JT, Giglio L, Collatz GJ, Kasibhatla PS, Arellano AF (2006). Interannual variability in global biomass burning emissions from 1997 to 2004. Atmospheric Chemistry and Physics, 6(11), 3423-3441

Weiss A, Hays CJ. Calculating daily mean air temperatures by different methods: implications from a non-linear algorithm. Agricultural and forest meteorology 128.1 (2005): 57-65

Werth PA, Ochoa R (1993). The evaluation of Idaho fire growth using the Haines Index. Weather and Forecasting, 8(2), 223-234.

Werth PA, Potter BE, Clements CB, Finney MA, Goodrick SL, Alexander ME. McAllister SS (2011). Synthesis of knowledge of extreme fire behavior: volume I for fire managers.

Westerling AL., Climate, Santa Ana winds and autumn wildfires in southern California. Eos 85.31 (2004): 289-296

Westerling AL, Swetnam TW (2003). Interannual to decadal drought and fire in the western United States. EOS, Transactions American Geophysical Union, 84(49), 545-555.

Westerling AL, Hidalgo HG, Cayan DR, Swetnam TW (2006). Warming and earlier spring increase western US forest fire activity. science, 313(5789), 940-943

Williams TM, Williams BJ, Song B (2014). Modeling a historic forest fire using GIS and FARSITE. Mathematical & Computational Forestry & Natural Resource Sciences, 6(2)

Yue X, Mickley LJ, Logan JA (2014). Projection of wildfire activity in southern California in the mid-twenty-first century. Climate dynamics, *43*(7-8), 1973-1991

Chapter 3. ESTIMATING WILDFIRE GROWTH FROM NOISY AND INCOMPLETE DATA USING A BAYESIAN STATE-SPACE MODEL

3.1 INTRODUCTION

Understanding and quantifying wildfire behaviors is of interest to the fire management and the research community for numerous reasons. Fire managers may want to know when wildfires will blowup to improve firefighter safety, gauge the effectiveness of firefighting strategies, or predict when and where large campaign wildfires are likely to occur. Researchers want to understand how wildfire behavior interacts with the environment, identify patterns of growth, or monitor trends. Quantifying wildfire behaviors will often use mathematical representations of growth, which can be broadly divided into physical and empirical models (Taylor et al. 2013). In either case, an obviously valuable piece of information is a complete and accurate record of fire growth over its lifetime, which can be used for a variety of purposes. For instance, growth data could be directly compared against predictions from currently existing wildfire theoretical and statistical models to validate their credibility and identify potential improvements (Andrews et al. 2007, Alexander and Thomas 2003, Taylor et al. 2013). Growth data from multiple incidents could also be used to better estimate the space-time distribution of wildfire emissions (Veraverbeke et al. 2015, Turquety et al. 2007, Mangeon et al. 2015) and associated health effects (Moeltner et al. 2013). Moreover, specific quantities that are calculated from burn area time series are often of interest to researchers and fire managers. Examples of these quantities include final burn area (Turetsky et al. 2004), area burned per day (Billmire et al. 2014, Birch et al. 2014, Turner et al. 1994), as well as the classification of high and low growth days (Finney et al. 2009).

Growth data may come from multiple sources, including written records of size and

spatially explicit burn area maps. Non-spatial records of burn area over time are typically obtained from case studies, historical and administrative records (Taylor et al. 2013). A commonly used non-spatial dataset are Incident Command System 209 (ICS-209) forms, which are compiled for important natural disasters occurring on federally owned lands in the United States. ICS-209 reports give near-daily updates of an incident's progression over time and are distributed to agency managers to provide the most current information. The information in turn assists with planning at broader geographic planning scales, like resource allocation and incident prioritization. An individual record contains 47 blocks of information including incident name, date and time, coordinates, management strategy, fuel types, values-at-risk, committed resources, estimated costs, containment dates and the incident size (Thompson 2013). While a complete daily burn area time series can sometimes be constructed from ICS-209 reports, they are not compiled for every incident, and frequently contain missing and erroneous entries.

Burn area time series can also be based on spatially explicit fire data sources, which are produced by a variety of state and national agencies (Short 2014). For instance, the Geospatial Multi-Agency Coordination (GeoMAC) produces near daily burn area perimeter maps for wildfires in the United States for fire managers, land managers and the public. GeoMAC burn area perimeter maps are constructed using a variety of information sources including geographic information systems specialists, GPS data, and IR imagery from fixed-wing and satellite instrumentation (Walters 2008). Other information sources used to produce burn perimeter maps include field-based intelligence, aerial imagery (Parks 2014, Kasischke et al. 2002) and satellite data (i.e. Landsat, MODIS, AVHRR) (Veraverbeke et al. 2014, Parks 2014, Li et al. 2004). Like ICS-209 reports, GeoMAC growth records often have at least one missing daily burn area measurement during the lifetime of an incident, may contain errors, and are not produced for

every fire. Burn area estimates from burn perimeter maps can be augmented using satellite hotspot data, which detects locations with anomalously high ground temperature globally, and consistently over time. The Hazard Mapping System (HMS) is an example of these kind of data. HMS detects the daily presence/absence of active burning on a 1-km^2 grid and is quality-controlled by human analysts who remove false alarms and add missing detects. Burn area estimates can be estimated from satellite hotspot detects, but they suffer from other data quality issues and often differ from burn scar estimates (Zhang et al. 2011).

While there are multiple sources of daily progression data, the quality of growth data can be poor (Taylor et al. 2013). ICS-209 reports are based on self-reporting by the incident team and may contain typographical errors (Calkin et al. 2014, Raffuse et al. 2009). Moreover, ICS-209 forms reflect the best available information at the time they are issued and mapping technology can change over a fires lifetime. Initial ICS-209 reports may be based on best guesses and overestimate the cumulative burn area (CBA). Later reports may have better mapping technology and decrease the burn area estimates, sometimes leading to a reported decrease in fire size. Spatially explicit data also have problems with data quality. GPS derived burn area perimeter maps might not map unburned patches of vegetation in the interior of burn areas for safety or practical reasons. The delineation of GPS derived burn area perimeters are also inherently subjective due to so-called fuzzy edges (Kolden and Weisberg 2009). Burn area estimates based on satellite hotspot detects have a number of sources of uncertainty. For instance, burn area estimates will be influenced by detection probabilities that are affected by vegetation (Tansey et al. 2008), clouds and smoke (Parks 2014), fire size (Raffuse et al. 2009) and low fire energy. Moreover, the burn area estimates from satellite hotspots can be inaccurate and are not always well validated (Zhang et al. 2011). Still, satellite burn area estimates can be helpful when burn

area measurements missing from written reports and progression maps (Thompson 2013, Mangeon et al. 2015). Hence, the burn area observations available to a given incident may be come from multiple sources, each with unique sources of error and data generating processes.

Clearly complete and accurate records of fire growth would be valuable to fire managers and researchers, however burn area data is likely incomplete and contains errors. There is then a methodological need to take a collection of burn area measurements taken throughout the fires lifetime, possibly from multiple sources, and output an estimated growth curve. Growth curve estimates could come from multiple methods. Missing entries in written records and burn perimeter maps could be interpolated using piecewise linear functions or using local smoothing techniques (Friedman et al. 2001), although outlier observations could result in unrealistic growth curves predictions and mask periods of extreme growth (Nakai and Ke 2011). Missing entries in burn perimeter maps can be reconstructed using machine learning techniques (Parks 2014), but does not explicitly deal with measurement error. Satellite hotspot data will not contain missing entries, but burn area estimates may be questionable and ignores information from other data sources. It is desirable of having a method of consolidating all available information about wildfire burn area time series into a single, realistic growth curve. Moreover, the method ideally should acknowledge that the accuracy of burn area measurements can change by data type and over the lifetime of the fire. In this chapter I propose a method of reconstructing wildfire growth curves using a Bayesian State-Space approach, which will generate samples of growth curves that were likely to have generated burn area observations over the fires lifetime. The reconstructed curves will assume a certain level of measurement error and will be constrained to prevent shrinking fires using a parametric model of growth. The reconstructions can incorporate multiple sources of wildfire growth data and borrow information from past fires. Hence, the

framework is able to incorporate a great variety of information about an individual wildfire's growth, while resolving a number of the issues that were raised earlier.

I will begin to explore the problem of reconstructing wildfire growth curves from incomplete and corrupted data in section 2.1, where I will describe how wildfire growth reconstruction can be accomplished in a Bayesian State-Space framework. In subsection 2.2 and 2.3, I will introduce two reconstruction models that I will use in this chapter and explain important constraints on the parametric models of growth. Subsection 2.4 discusses how the models assume burn area observations are related to the growth curve predictions. Subsection 2.5 describes how the growth model and observations interact in the final Bayesian State-Space framework. I will close this section with an explanation of ways that important prior information can be incorporated in this framework. In section 3, I will apply the reconstruction models to growth data from 13 wildfire incidents in the United States. Subsection 3.1 will introduce the two types of burn area data that will be used in an application of the framework and subsection 3.2 will be devoted to describing how the remainder of priors was constructed. Subsection 3.3 will explain the computational details related to the application of the proposed reconstruction models. Section 4 will summarize the mathematical and computational results of the application of the reconstruction model to real-world data. Section 5 will report the results of an informal prior sensitivity analysis that compares the effects of substituting priors on a typical growth curve. I close the paper in section 6 by discussing the utility the modeling framework as a tool for data reconciliation, generating realistic fire growth trajectories and evaluating key facets of fire behavior.

3.2 MODEL DEVELOPMENT

3.2.1 *Conceptual model*

The Bayesian state space approach requires identifying a suitable process model that represents the true CBA. CBA measurements are typically reported at a daily step, suggesting that a discrete-time growth model would be appropriate. Given known aspects of fire behavior, it will be assumed that the CBA for any fire may not be negative or infinite, and that CBA can never shrink. It also natural to assume that CBA is an additive function of the cumulative changes in burned area during each day in which a wildfire is active. The total area burned is, therefore, the sum of the difference in area burned from each day of the incident to the next. Using this conceptual model, the Beverton-Holt difference equation was identified as a good parametric model of an individual wildfire's CBA that avoided pathologies that occur in related models (May 1976). If X_t defines an incident's CBA on day t, then the growth model would be of the form,

$$X_t = \frac{r_{t-1} K X_{t-1}}{K + (r_{t-1} - 1) X_{t-1}}.$$

Here r_t is the inherent growth parameter on day t, K is the eventual burn area and X_0 is the initial condition (Beverton and Holt 1957, De la Sen 2008). The assumptions of the conceptual model are satisfied by choosing $K > X_0 > 0$ and $r_t \geq 1$. The growth curve will begin at the initial value, X_0, and asymptotically approach the final burn size, K, as $t \to \infty$. Larger values of r_t will correspond to faster growth than smaller values of r_t. To simplify the framework, I define $K = 1$, so the process state corresponds to the true cumulative *percentage* burned.

3.2.2 *Stationary and non-stationary process*

Two versions of the framework will be explored in this chapter. The stationary version will set the inherent growth parameter to a constant, which will produce an idealized wildfire growth curve that can be interpolated by a logistic curve (Beverton and Holt 1957). Since only one parameter describes the distribution of growth over the wildfire's lifetime, it is a useful summary growth statistic. On the other hand, it may be desirable to have a realistic reconstruction of the day-to-day growth of a wildfire. For realistic growth reconstructions, I propose a non-stationary version of the framework and let,

$$r_t - 1 = (r - 1)\omega_t.$$

where ω_t is lognormal white noise with geometric mean one and geometric standard deviation τ. Hence, the variance forced into the inherent growth parameter is controlled with the τ parameter and its average is controlled with r. Using a multiplicative random walk on the shifted inherent growth parameter forces $r_t \geq 1$, prohibiting decreasing growth curves. Note that for a process time series of length T, the last value of the inherent growth parameter, r_{T-1}, is arbitrary and I set $X_T = 1$.

3.2.3 *Initial conditions*

In addition to the inherent growth parameter, the process model must be initialized at a non-zero wildfire size at day zero. It is convenient to instead think of the initial conditions in terms of time until the maximum daily growth. For the stationary model, the day of the largest blow-up, i.e. $\text{argmax}_t\{X_t - X_{t-1}\}$, is forced to an integer $t_{max} \geq 1$, by initializing at $X_0 = (1 + r^{t_{max} - 1/2})^{-1}$. Assuming that the largest blow-up occurs within the observation window implies that $1 \leq t_{max} \leq T - 1$ or $\frac{1}{1+r^{1/2}} < X_0 < \frac{1}{1+r^{T-3/2}}$. Extending t_{max} to non-integer values is equivalent to

shifting the location of the logistic curve that interpolates the process state time series. Note that for the non-stationary model, in spite of the above initialization procedure, the largest daily change in size may not occur on day t_{max} due to daily variability in the inherent growth parameter.

3.2.4 *Observation equations*

It is assumed that burn area observations are noisy but unbiased realizations of the parametric growth model. Since the burn area of a fire is a statistic that must be greater than zero, it makes sense to assume multiplicative rather than additive errors. It is natural to assume that the errors will be larger when the fire is rapidly growing than when it not growing. The model captures the assumed heteroscedasticity by probabilistically linking the observations and true burn area via,

$$Y_{it} \sim \text{Lognormal}(\ln(K_i X_t), \sigma\sqrt{\frac{X_t}{X_{t-1}}}).$$

Here K_i represents the asymptotic final burn area for data type i and σ is the geometric standard deviation of the observation errors when the fire is not growing. Y_{it} and X_t are the observed and true CBA for data type i at time t.

3.2.5 *Bayesian State-Space framework*

The parametric growth model is related to burn area observations through a slight variation of the Markovian state-space framework.

$$X_t = f(\boldsymbol{\theta}, X_{t-1});$$

$$Y_{it} = g_i(\boldsymbol{\gamma}, \quad X_t, \quad X_{t-1}).$$

X_t is the process state that represents the true CBA of the incident at the discrete time point t. The process state is defined with growth model, f, which accepts a vector of parameters $\boldsymbol{\theta}$. The observation equations, g_i, establishes the probabilistic relationship between the process state, X_t,

and the corresponding observed CBA from data type i, Y_{it}. The observation equations accept the parameters in vector $\boldsymbol{\gamma}$ (Godsill et al. 2004). For the stationary and non-stationary models $\boldsymbol{\theta} = (r, X_0)$ and $\boldsymbol{\theta} = (\boldsymbol{r_{0:T-2}}, X_0)$ respectively. The observation equations are the same for both frameworks, accepting one parameter that controls the observation error and a final burn area parameter for each data type.

3.2.6 *Process level priors*

The prior probability distribution of r was constructed by exploiting the fact that under the stationary model, $r = (m+1)^2/(m-1)^2$, where $m = \max_{X_0}\{X_1 - X_0\}/K$. In words, m is the percent of final growth that occurred during the largest daily growth increment and is referred to as peak growth. Peak growth was calculated for 2,013 wildfires using ICS-209 records from 2002-2013 (unpublished data) and a beta distribution was fit via maximum likelihood. The same initial conditions prior, $X_0 \sim \mathrm{U}\left(\left(1 + r^{1/2}\right)^{-1}, \left(1 + r^{T-3/2}\right)\right)$, was used for both frameworks, which constrains the growth curve such that largest daily increment in size occurred within the fires lifetime. The non-stationary framework requires an additional prior for τ, which controls the geometric standard deviation of the inherent growth parameter. The noise prior was constructed by considering two extreme process variability scenarios that define the central 90% interval of the distribution. To set the lower percentile on the τ prior, two near identical levels of peak growth growth, m_1 and m_2, were considered. The values corresponded to specific values of $r_1 - 1$ and $r_2 - 1$, which differed by a multiplicative factor. I identified the level of τ_5 such that the probability of a multiplicative change this extreme is 0.002. The quantities $m_1 = 1/1585000$ and $m_2 = 1/1585001$ represent near identical values of m and were used to calculate the τ_1, which defined the 5th percentile of the τ prior. The 95th percentile was calculated using a

similar process but with two very dissimilar levels of percent growth, $m_1 = 1/1000$ and $m_2 = 1/1585001$. The multiplicative difference between $r_1 - 1$ and $r_2 - 1$ was calculated and I identified the level of τ_{95} such that the probability of the difference or greater is 0.2.

3.3 APPLICATION

3.3.1 *Data sources and pre-processing*

To illustrate how both models can be applied, wildfire growth data from 13 incidents from the 2014 wildfire season were collected from two databases: GeoMAC fire perimeters and Hazard Mapping System hotspot detects (HMS, ftp://satepsanon.nesdis.noaa.gov/volcano/FIRE/Anca/, Acquired February 2015). The cumulative number of actively burning HMS pixels will be used as a proxy for CBA over time.

In this application, for an individual incident k, there are two corresponding observation vectors, which are T_k elements long, where T_k is the number of days between the first and last GeoMAC perimeter and a six day buffer period. A temporal buffer of three days was appended before the first and after the last GeoMAC perimeter to record any HMS detects that fall outside the lifetime of range of GeoMAC measurements. Each vector is populated with CBA estimates from each of the two data types. The GeoMAC CBA estimates were extracted from the "area" feature from each of fire perimeter. Where two perimeters existed on the same day, only the perimeter with largest area was kept. The HMS CBA estimates were set as the percentage of total HMS hotspot detects occurring within the incident boundary. The incident boundary was defined to be the largest GeoMAC perimeter including an 8-kilometer buffer. The data are assumed to be a proxy for the percentage of total biomass burned by incident k at time t. HMS entries with zero cumulative hotspot detects were labeled missing and GeoMAC observations

were labeled missing if no polygon was recorded for that day.

3.3.2 *Observation level priors*

Realistic bounds were placed on the geometric standard deviation, σ, as to represent the full range of possible errors. The upper bound describes a scenario where there is a 5% probability of a multiplicative error of greater than or equal to a factor of 10. The combined frequency and magnitude of errors in the upper bound scenario is not something that should be expected in most CBA data and represents an extreme worst-case scenario. An error of that magnitude would most likely be a transcription error, which are relatively rare, and the 5% probability would imply that an average 5% of the days would have this level of error or greater. To further illustrate how extreme the upper bound scenario would be, I surveyed eight ICS-209 reports where the CBA was overestimated and then corrected on the subsequent report. The largest overestimate was by a factor of 1.8, but factors less than 1.05 were much more common. The lower bound was set such that the probability of a multiplicative error greater than or equal to a factor of 1-1/1,585,000 was 5%. The lower bound scenario represents a case where observations from Yellowstone fires would be recorded at a spatial resolution that was less than an acre, which is an unrealistic level of accuracy given the issues outlined in the introduction and the scale that CBA measurements are reported. The upper and lower bound scenarios correspond to the endpoints of a uniform distribution.

The model also requires a prior on the final burn area, K_{GeoMAC}, for the GeoMAC data. Final burn area measurements were recorded in hectares using the same 2,013 ICS-209 records and were transformed using $Z = \ln\left(\frac{BA}{404}\right)$. A generalized gamma distribution was fit to the transformed measurements using maximum likelihood. Where applicable, QQ-plots were visually inspected to verify that the distribution adequately described the empirical data

(Appendix A).

3.3.3 *Estimation*

Combining all the process and observation level components completes the Bayesian hierarchical framework formulation (Table 3.1).

Table 3.1 Formulation of the both state-space models

Growth model	f	$\frac{r_{t-1}X_{t-1}}{1+(r_{t-1}-1)X_{t-1}}$
Stationary priors	$\boldsymbol{\theta}$	$m \sim \text{Beta}(2.37,1.65)$ [a] $X_0 \sim U(\frac{1}{1+r^{1/2}}, \frac{1}{1+r^{T-3/2}})$
Non-stationary priors	$\boldsymbol{\theta}$	$\tau \sim \text{Lognormal}(-6.827,5.214)$ [b]
Observation equations	g_i	$Y_{it} \sim \text{Lognormal}(\ln(K_i X_t), \sigma\sqrt{\frac{X_t}{X_{t-1}}})$
Observation priors	$\boldsymbol{\Upsilon}$	$\sigma \sim U(3.219\times10^{-7}, 1.175)$ $\ln(K_{GeoMAC}/404) \sim \text{Gen. Gamma}(0.396,0.298,2.357)$ $K_{HMS} = 1$

[a] - $r = (m+1)^2/(m-1)^2$

[b] - $\tau = \text{SD}(\ln(r_{0:T-2} - 1)$

Both the stationary and non-stationary frameworks were fit using Just Another Gibbs Sampler (JAGS) software and the runjags package in R (R Development Core Team 2008) on a MacBook Pro with a 2.7 GHz Intel Core i7 processor. An initial Markov Chain Monte Carlo (MCMC) was computed using three parallel chains with a nominal sample size of 1000 and thinning interval of 100. The chains had a burn-in period and adaptive phase of 10000 iterations. Convergence was monitored visually and by calculating the potential scale reduction factor (PSRF), of the range of the 5^{th} and 95^{th} percentile of the marginal posteriors (Brooks and Gelman 1998). The second half of the chain was assumed to have approximately converged if the maximum PSRF convergence diagnostic fell below 1.01. If the chain had not converged, then it was extended in batches of 1000 iterations until the maximum PSRF diagnostic was less than 1.01 (Gelman and Shirley 2011).

3.4 RESULTS

The stationary framework was computationally cheaper than the non-stationary model both in terms of iterations required until convergence and sampling efficiency (Table 3.2). The slowest converging application of the stationary framework still completed in substantially less time than any application of the non-stationary framework. Longer duration wildfires tended to require more time per Gibbs iteration than shorter duration events. With the exception of the Somers fire, the increased costs of the non-stationary framework are compensated by a noticeably improved reconstruction of the observed data (Table 3.3). The improvement in model fit is also apparent when graphically comparing the stationary and non-stationary reconstructions to the data (Figures 3.1-3.2). The stationary growth curves assumed a smooth progression from ignition to containment, while the non-stationary permits variable growth over the fires lifetime, allowing pauses in wildfire growth and sudden bursts of activity.

Table 3.2 Computational requirements

Firename	Iterations until convergence (×1000)		Iterations per second		Total time	
	S	*NS*	*S*	*NS*	*S*	*NS*
a.) Beaver	3	9	61	2.0	49	4517
b.) Big Cougar	1	77	111	8.8	9	8715
c.) Buzzard	3	8	129	10.2	23	785
d.) Carlton	3	18	70	2.5	43	7284
e.) Devils Elbow	2	64	107	4.7	19	13561
f.) Eiler	2	46	97	3.9	21	11655
g.) French	3	36	93	3.9	32	9328
h.) Happy Camp	1	6	35	1.1	28	5364
i.) Johnson Bar	2	13	34	0.6	59	22659
j.) King	2	20	57	1.8	35	11186
k.) Snag Canyon	2	84	73	2.6	27	32475
l.) Somers	1	5	82	6.0	12	833
m.) South Fork	3	23	41	0.8	74	27803

Table 3.3 Log Bayes factor, number of observations and final burn area

Firename	$2\ln(BF)$	N_{GeoMAC}	N_{HMS}	K_{GeoMAC}
a.) Beaver	215.3	25	38	13139
b.) Big Cougar	27.1	12	18	26397
c.) Buzzard	20.5	9	19	159992
d.) Carlton	92.3	21	33	104731
e.) Devils Elbow	66.8	11	24	9751
f.) Eiler	83.6	15	26	13426
g.) French	64.0	15	26	5611
h.) Happy Camp	201.2	45	53	54782
i.) Johnson Bar	247.8	29	69	5383
j.) King	48.0	30	37	39295
k.) Snag Canyon	149.3	23	31	5169
l.) Somers	0.3_a	17	26	14644
m.) South Fork	39.9	27	58	26780

[a] Negligible improvement using non-stationary (Kass and Raftery 1995)

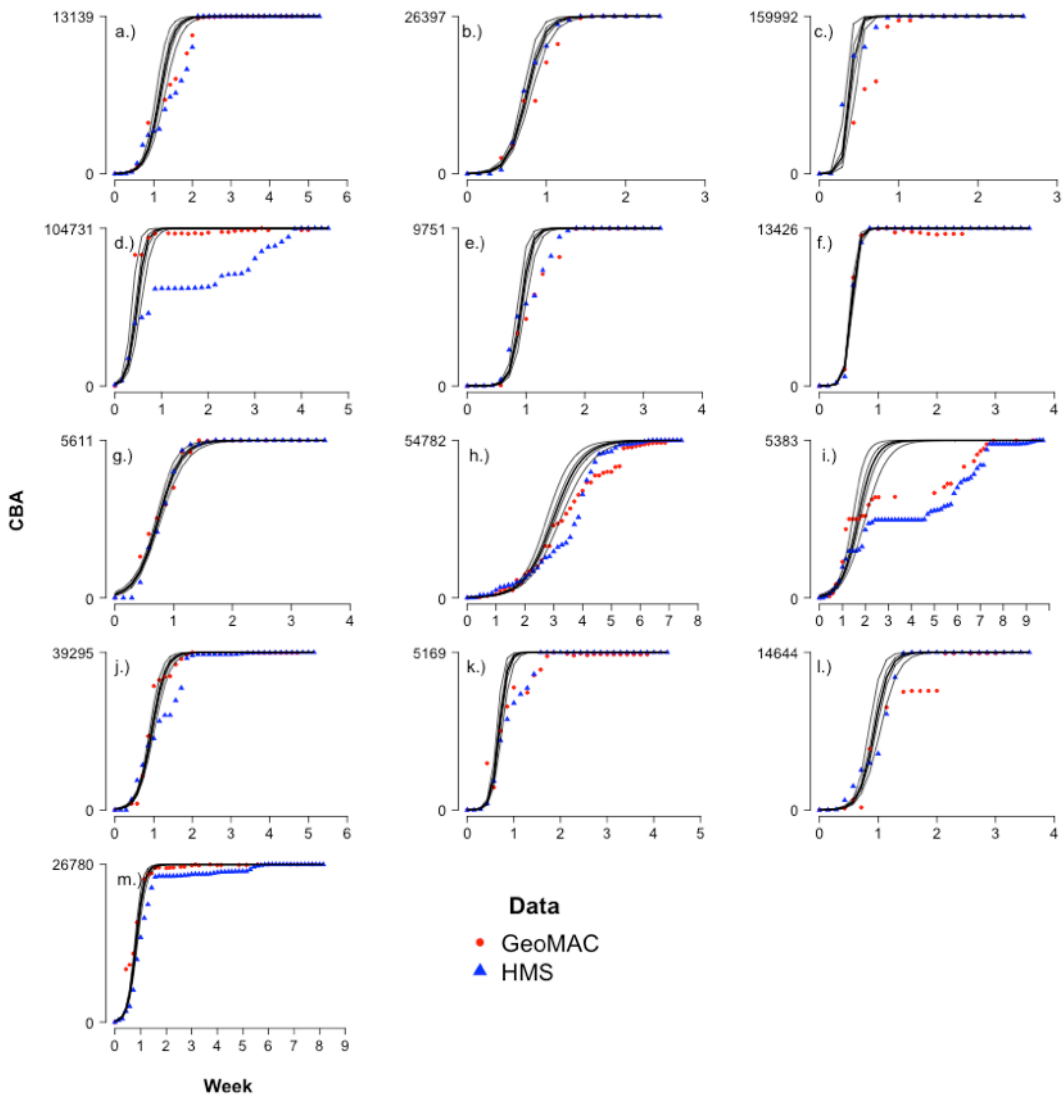

Figure 3.1 The GeoMAC burn area estimates and percent of total HMS burn area measurements are shown as red and blue points, respectively. The 2.5,25,50,75 and 97.5th percentile of the stationary model's marginal posterior distributions for the process state over time are shown as solid curves, the median is the thick curve. Letters correspond to the wildfire incidents in Table 3.2.

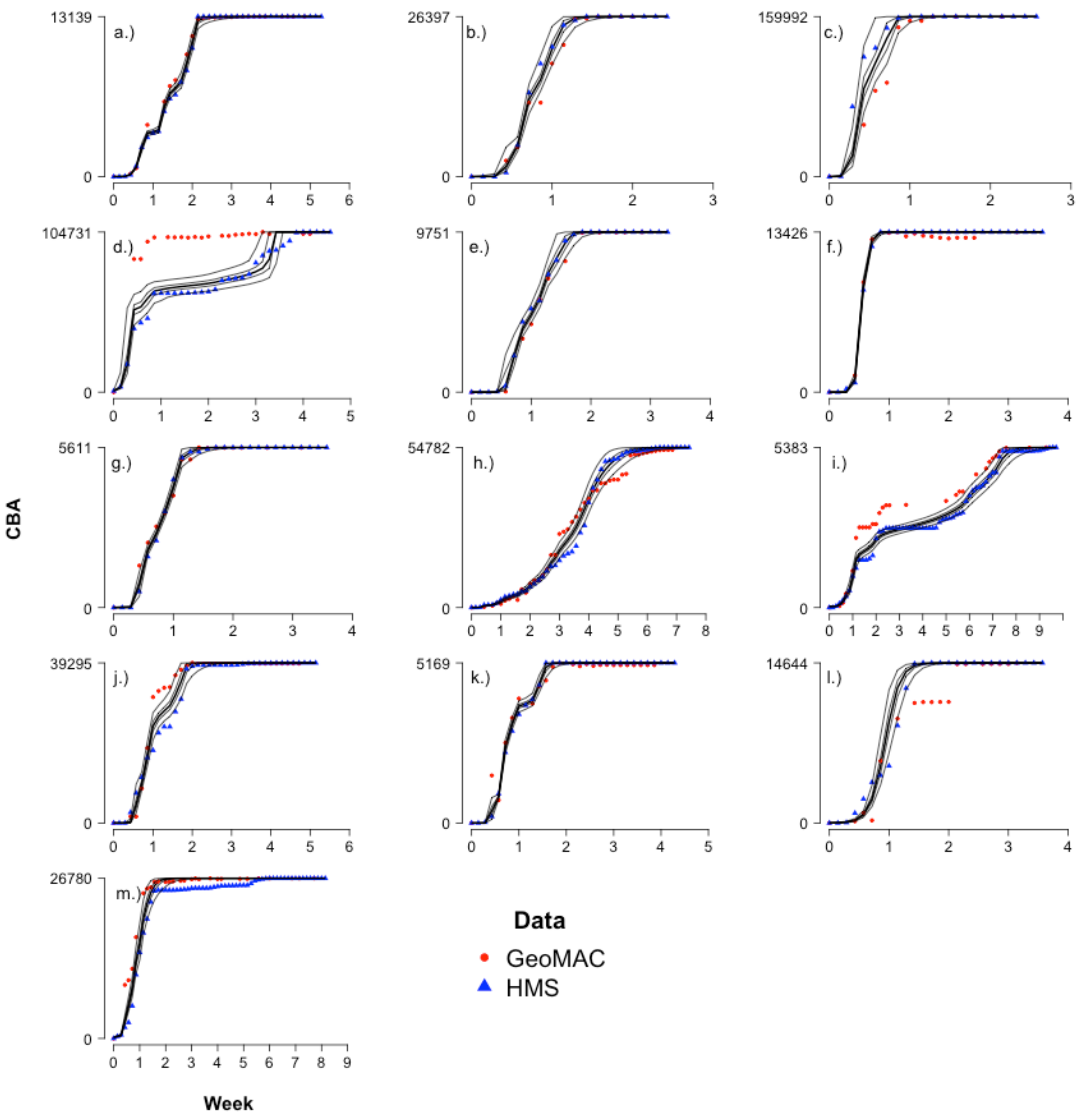

Figure 3.2 The GeoMAC burn area estimates and percent of total HMS burn area measurements are shown as red and blue points, respectively. The 2.5,25,50,75 and 97.5th percentile of the non-stationary model's marginal posterior distributions for the process state over time are shown as solid curves, the median is the thick curve. Letters correspond to the wildfire incidents in Table 3.2.

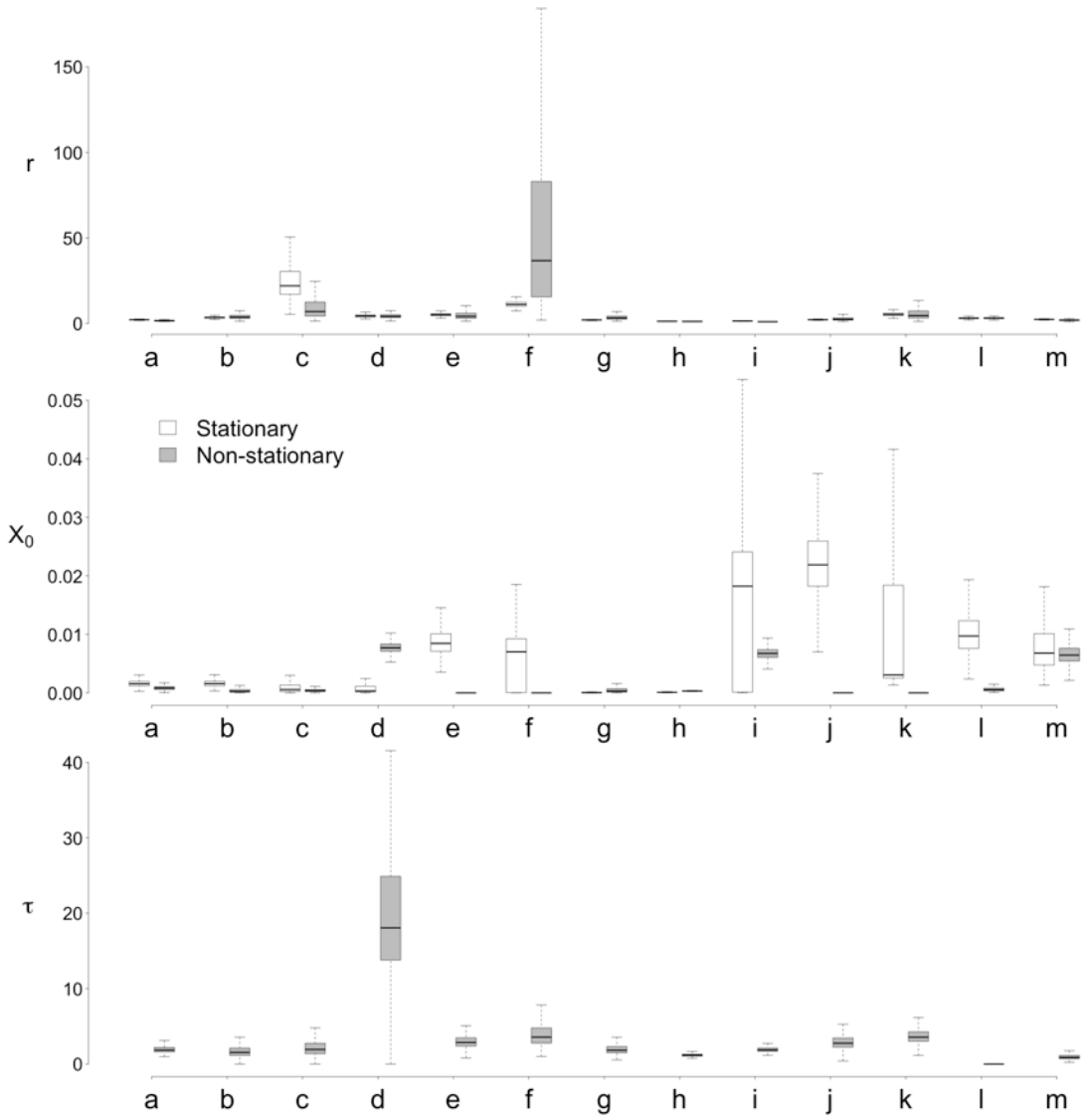

Figure 3.3 Boxplots of each process level parameter's marginal posterior for each framework and fire. Process level parameters included the inherent growth parameter (Top); initial conditions (Middle) and the geometric standard deviation of the inherent growth parameter (Bottom) are shown. Outliers were omitted to improve the visibility. Letters correspond to the fires in Table 3.2.

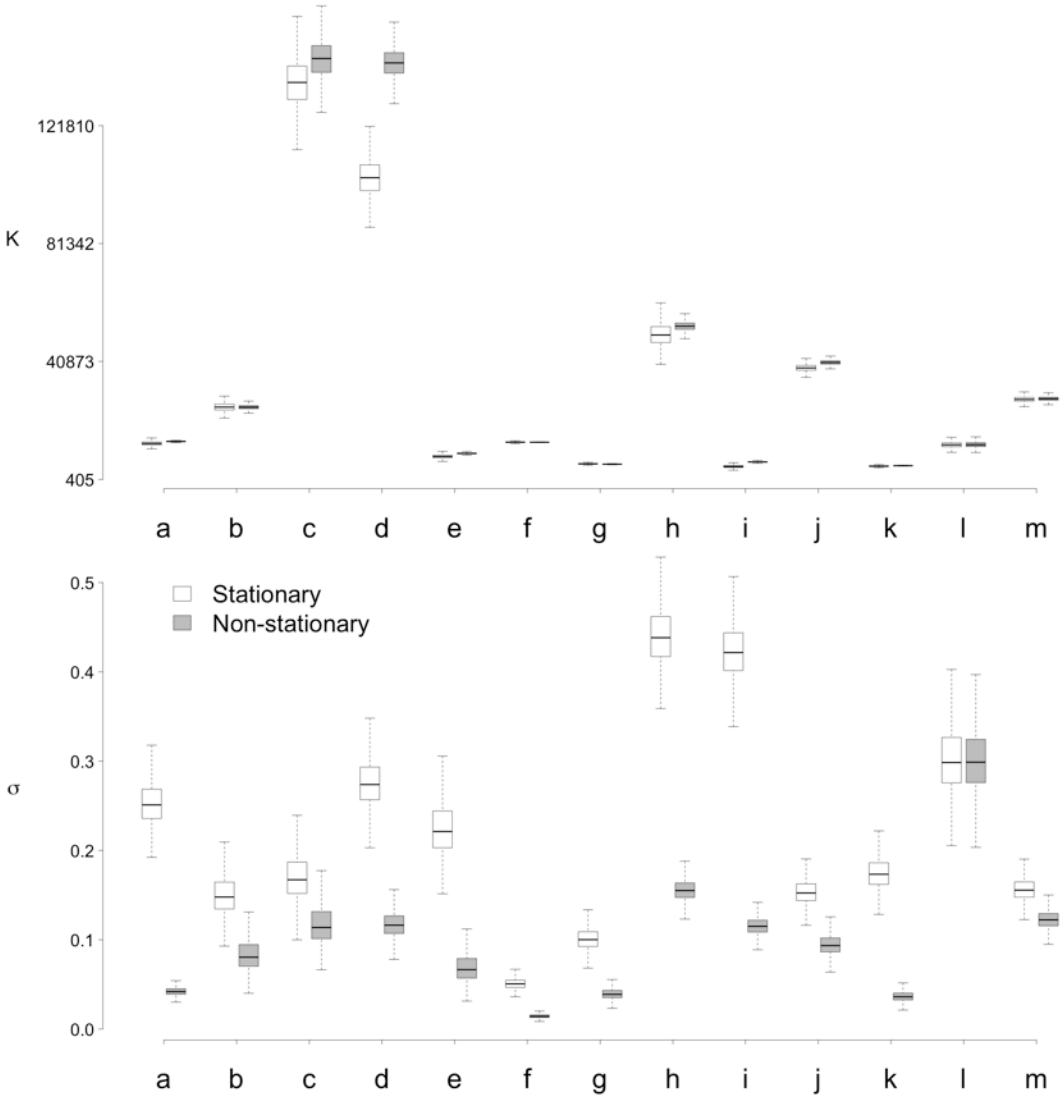

Figure 3.4: Boxplots of each observation level parameter's marginal posterior for each framework and fires. Observation level parameters included the final burn area for GeoMAC (Top) and observation error (Bottom). Outliers were omitted to improve the visibility. Letters correspond to the fires in Table 3.2.

The estimates and variability of the inherent growth parameter were altered by the choice of reconstruction framework. For instance, the median inherent growth parameter for the Buzzard wildfire was higher in the stationary framework than in the non-stationary, but the reverse was true for the Eiler wildfire. The median initial conditions tended to be higher in the stationary framework than the non-stationary framework and the uncertainty in the estimates was often larger in the stationary reconstructions. For the non-stationary framework, the noise forced into the inherent growth parameter, τ, also showed noticeable variability between incidents. A few incidents had extremely low process variability and were nearly stationary, which was seen in the Somers fire. The Somers fire had a median and interquartile range of τ of 4.4×10^{-4} and 8.1×10^{-3}. In contrast, τ was occasionally estimated to be relatively large, as was seen in the Carlton fire. The level of uncertainty in the estimates of τ also varied substantially between incidents (Figure 3.3). The median posterior of τ was 1.9, but could be near zero or almost as high as 20. The estimates and uncertainty of K_{GeoMAC} were usually similar in both the stationary and non-stationary frameworks; although the Carlton fire was a notable exception. The mean and variance of the observation error tended to be higher in the stationary framework (Figure 3.4).

In general, applying the stationary framework will require at most a few minutes to converge, outputting a sample of daily growth curves that approximate the posterior. The fit of the stationary model may be adequate for short duration fires, although the non-stationary model typically improved the fit. The non-stationary framework took longer to complete than the stationary framework, taking anywhere from 13 minutes to 9 hours to finish. Computer time seemed to in part be related to the wildfire duration, and the slow convergence of measurements near the beginning and end of the reconstruction.

3.5 SENSITIVITY ANALYSIS

3.5.1 *Overview*

While the prior distributions were constructed in an objective and reasoned way, it is likely that another analyst may propose others given their personal knowledge and experience. It is valuable then to quantify how the results will change if the prior distributions are changed. One method of accomplishing this is by reapplying the framework with new priors and monitoring how the posteriors are changed. New prior distributions will then be proposed for K, m, σ and τ and used to reanalyze the Johnson Bar fire. The Johnson Bar fire was used as a case study as it represents a situation where day-to-day growth varied over time, having a two-humped curve.

3.5.2 *Final burn area*

The final burn area model component was reanalyzed using a set of five priors. Two of the priors were constructed using simple assumptions about the bounds of the data while the remaining three were calculated from burn area data from the Monitoring Trends in Burn Severity project (MTBS, http://www.mtbs.gov, data acquired April, 2013). The data covers the conterminous U.S. and from the years 1984-2013. Fires smaller than 404 ha were removed from the dataset. The first bounded distribution will be called the lower-truncated inverse-uniform (LTIU) prior, which is just, $404\times K^{-1}\sim \mathrm{U}(0,1)$. The LTIU prior sets no upper limit on final burn area but constrains it to be greater than 404 ha in a very simple way. A second data driven variation will be called the lower-truncated inverse-beta (LTIB), which is just $404\times K^{-1}\sim \mathrm{Beta}(0.964,1.152)$, where the shape parameters are estimated via maximum-likelihood using the rescaled burn area data. Given that analysts are working in a finite spatial domain, one may wish to include an upper-truncation point on the final burn area parameter. Strict upper and lower limits can be

incorporated by using the bounded inverse-uniform (BIU) and bounded inverse-beta distribution (BIB). The BIU is just $K^{-1}\sim \mathrm{U}(1.56\times10^{-6}, 404^{-1})$, where the lower-bound represents a final burn area equivalent to the 1988 Yellowstone fires. Like the LTIB distribution, the shape parameters (0.958,1.149) for the BIB was fit from shifted and scaled burn area data using maximum-likelihood. The last final burn area prior was a Pareto(404, 1.13).

3.5.3 *Peak growth*

The peak growth component, m, will be reanalyzed using a set of four priors including the uniform (U), Mode-zero triangle (MZT), Mode-one triangle (MOT) and Arcsine distribution. Each of the distributions are special cases of the beta distribution with the following shape parameters, $m_U\sim\mathrm{Beta}(1,1)$, $m_{MZT}\sim\mathrm{Beta}(1,2)$, $m_{MOT}\sim\mathrm{Beta}(2,1)$ and $m_{Arcsine}\sim\mathrm{Beta}(0.5,0.5)$.

3.5.4 *Observation error*

In section 3.2, the prior was constructed for the observation error by defining what would be considered an extreme level of error and then finding the value of σ_{max} such that the probability of exceeding that level is 5%. This worst-case scenario is then used to set the upper bound of the prior on σ. The extreme level of error described in section 3.2 should be very rare but it is admittedly difficult quantify. Hence, it is desirable to gauge how robust the results are to changes in the value of σ_{max}. Hence, the case study will be reconstructed using various changes to the upper-truncation points of the observation error. Specifically, the upper-truncation points will be recalculated under small (1%,) medium (10%) and high (50%) probabilities of exceeding the extreme scenario.

3.5.5 *Process error*

The various levels of process error priors were constructed in much the same way as section 5.3. In section 2.6, two extreme cases of process error, one very-high and one very-low were used to define the 5th and 95th percentiles of the lognormal prior. The same process was repeated using low, medium and high levels of certainty, with the two extreme cases defining the $(\frac{\alpha}{2}, 1-\frac{\alpha}{2})$ percentiles of the τ prior for $\alpha = 0.01,0.05$ and 0.5.

3.5.6 *Analysis*

In the stationary model, the posterior of the Johnson bar reconstruction did not appear to be drastically altered in when the prior distribution was replaced (Figure 3.5). The largest change happened when the final burn area prior was replaced with the LTIU distribution, which reduced the posterior mean by 4 percent.

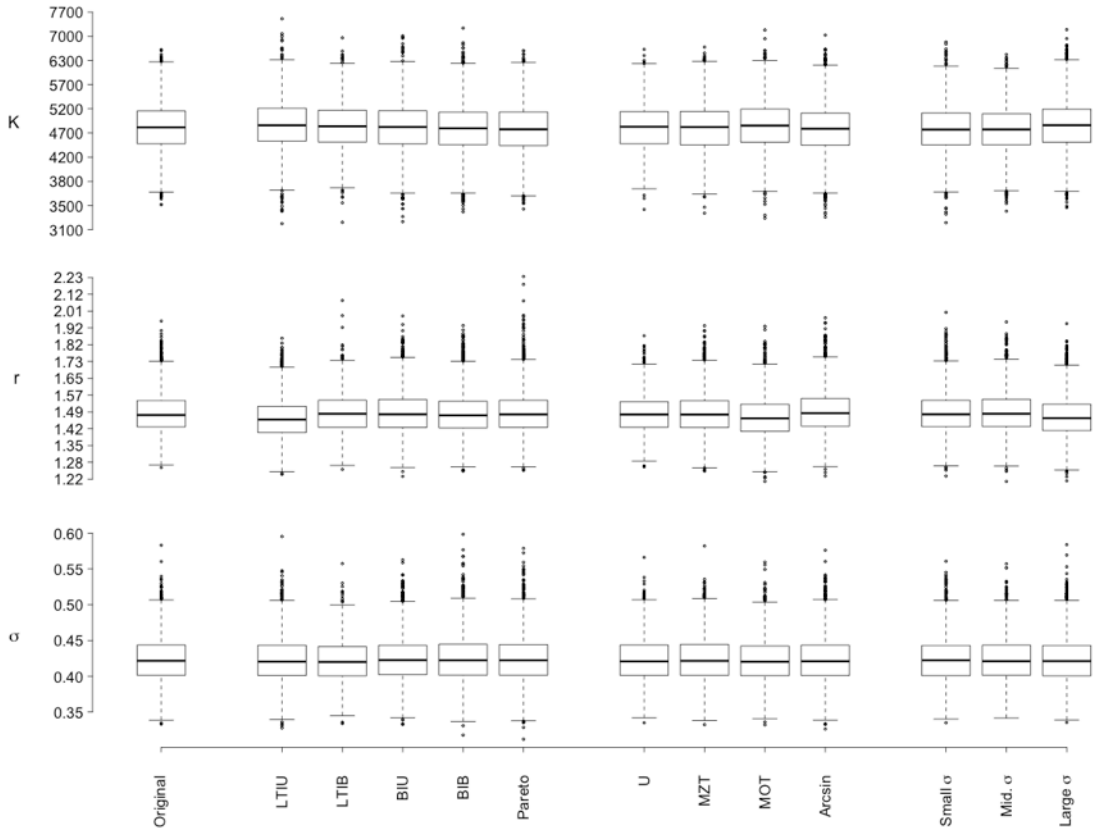

Figure 3.5 Marginal posterior distribution for each of the stationary model parameters.

The x-axis labels describe the changes that are made to the prior distribution.

In the non-stationary model, the posterior distribution of the Johnson bar reconstruction was also relatively invariant to changes in the prior (Figure 3.6). The largest change was seen when the inherent growth parameter prior was replaced with the MOT distribution, reducing the process error by 2 percent. The median growth curve reconstruction itself was also fairly robust to changes in the prior distributions. The largest change in the reconstructed curve happened on the first day when the inherent growth parameter prior was replaced with an arcsine distribution, increasing the estimated CBA by about 1 percent. The differences in the reconstruction reduced after this point and seemed to decay to near-zero levels in the last days of the reconstruction (Figure 3.7).

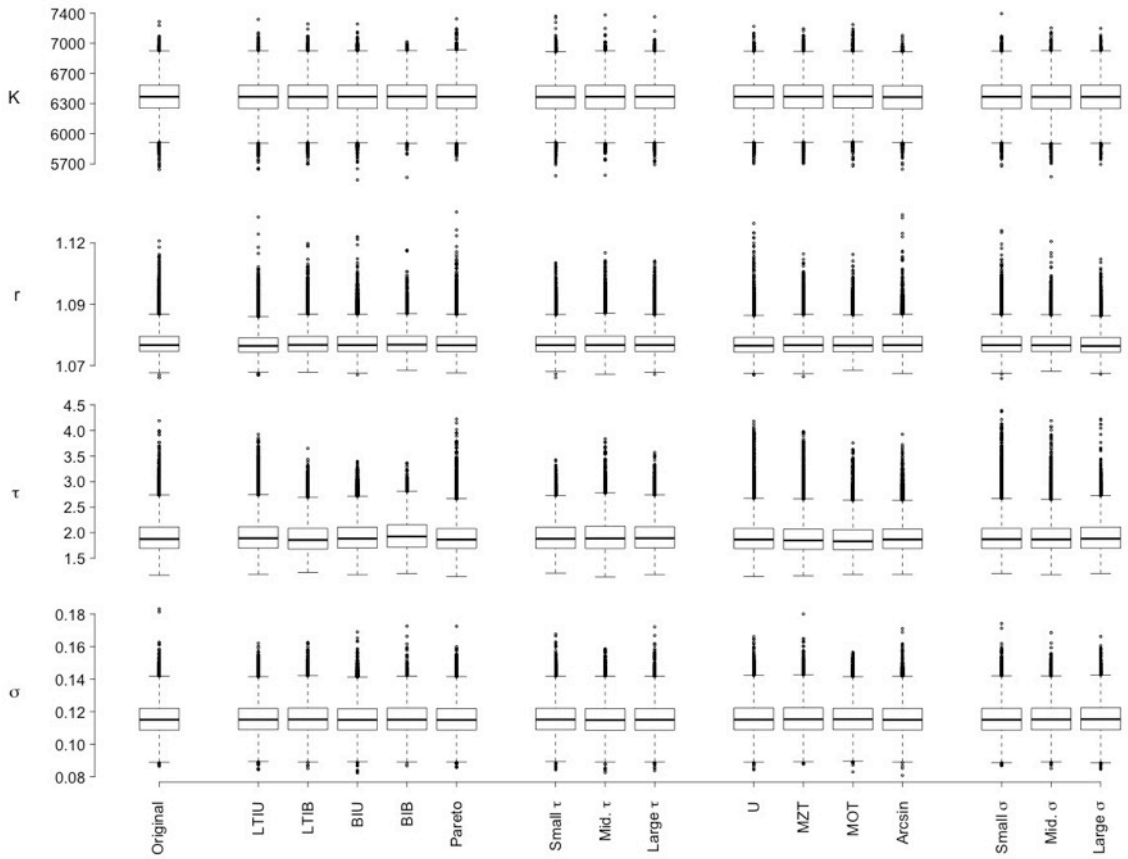

Figure 3.6 Marginal posterior distribution for each of the non-stationary model parameters.

The x-axis labels describe the changes that are made to the prior distribution.

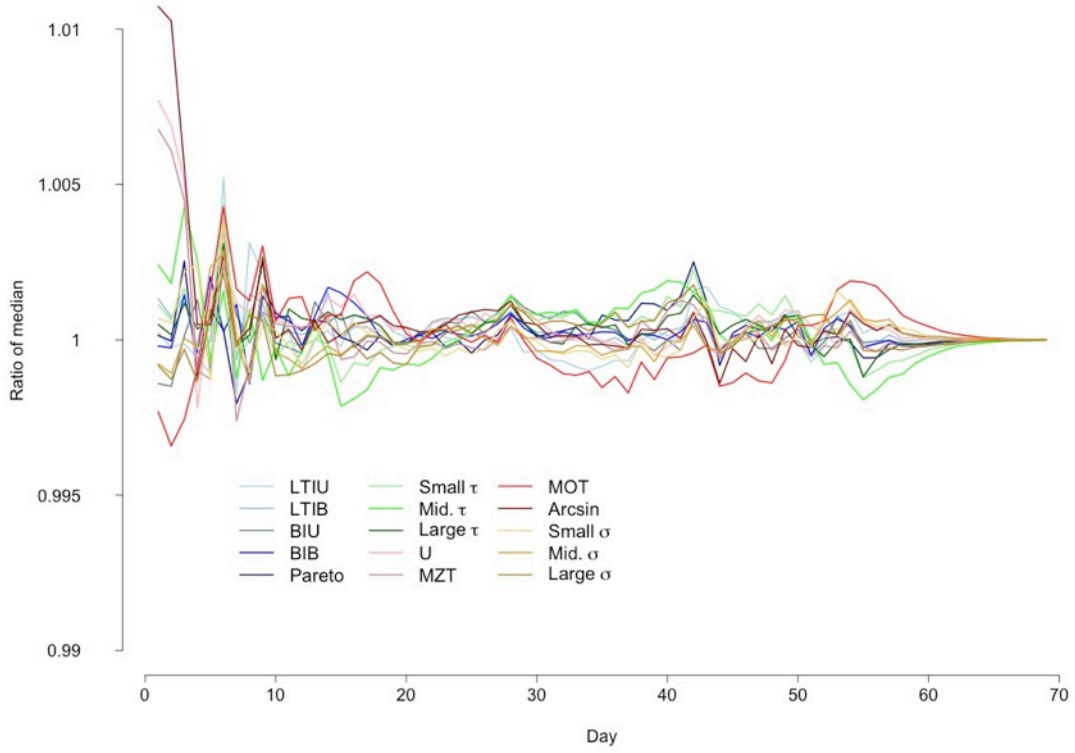

Figure 3.7 The ratio of the original (Figure 3.2j) and altered median growth curve reconstruction. Values greater than one correspond to CBA estimates that are larger than the original.

3.6 DISCUSSION

A variety of techniques could be used to generate complete growth curves from incomplete and corrupted burn area time series, ranging in complexity from simple imputation techniques (Nakai and Ke 2011), rule-based reconstructions (Zhang et al. 2011, Raffuse et al. 2009, Parks 2014), to complex physics-based simulations (Williams et al. 2014). However, the Bayesian state space models presented here is a unique approach to obtaining complete burn area time series and has a number of desirable features.

One obvious advantage to the state space approach is that the reconstructions are constrained to generate realistic growth curves, which is accomplished in at least two ways. Firstly, the choice of growth model generates curves that will conform to the conceptual model of wildfire growth and prevents fires that decrease in size. Secondly, the model is able to incorporate prior information about what types of growth curves should be expected based on measurements that are easily calculated from daily burn area time series. The state space approach easily incorporates burn area estimates from multiple sources, which will better model the uncertainty in the growth curve estimates. Measurement errors are explicitly modeled using equations that represent the unique data generating process of each data source. The output of the model is statistical, communicating the certainty of the estimates, and interpretable; the posterior of growth curves are the distribution curves that are likely based on burn area observations and prior evidence of what curves would be typical.

Given the value of burn area time series to scientists and fire mangers, a potentially useful application of the reconstruction models would be the construction of a wildfire growth curve database. The idea would be to aggregate all available data sources concerning an individual wildfire incident, and then obtain the highest quality reconstruction using the state

space model. Since realism of the growth curve would be desired, the non-stationary model would likely be used here. The growth curves database could be inputted into smoke forecasting tools, like BlueSky, to better model the uncertainty in burn area measurements (Raffuse et al. 2009). The reconstructed growth curves could also be used to validate currently existing growth models (Taylor et al. 2013), or calculate quantities that are important to fire managers and researchers like final burn area.

The framework is easily modified and alternative formulations could be used for other applications. Important environmental relationships could be linked to daily fire growth by letting the inherent growth parameter be a function of environmental variables. Future burn area time series can be forecasted by inputting incomplete burn area time series and relaxing the constraints on the initial conditions so that peak growth may occur outside the length of the time series. The final entries of burn area time series often repeat the same measurement many times and defining an extinguishment date can be difficult. Including an additional parameter that extinguishes the process at some time during the time series can be used to predict the extinguishment date, as well as quantify the uncertainty. Priors and growth models can be substituted to use the reconstruction model in other applications when observations are generated from a discrete time, monotonically increasing growth process.

While two frameworks of varying complexity were presented, either framework could be appropriate depending on the intended application. If only a crude model of wildfire growth is needed, then the stationary framework could be used to quickly summarize progression data with a few parameters. On the other hand, if the day-to-day changes in growth are of particular interest and a realistic growth reconstruction is required, then the non-stationary model would be the better choice. The drawback of latter is that the increased realism comes at the cost of overall

increased computational requirements. Reductions in computational cost can be dealt with strategically by noting that marginal convergence of process state tended to be slower at the beginning and end of the time series where there was little to no information about the fire's size. Modifying the model to include including an additional parameter that extinguishes the fire could reduce the computational burden by reducing the number of parameters describing this region of the time series. Applying the stationary model for short duration fires may provide an adequate description of the data at a very-low computational cost. Moreover, reductions in computational effort can also come from using efficient sampling algorithms, like Hamiltonian MCMC algorithms (Neal 2011).

While a large suite of variations to the original reconstruction model were examined in the sensitivity analysis, other aspects of model configuration could also be changed that can alter the resulting growth curves. Examples of potential changes include incorporating day-to-day variation in the inherent growth parameter using a multiplicative random walk, introducing parameters that force the growth curve to be extinguished, using different growth models, or assuming that the influence of growth is multiplicative on the standard deviation rather than the variance. Understanding how the reconstruction results are influenced by these changes could improve the reconstruction realism, goodness-of-fit, and computational burden. In addition to exploring the effects of changes to the model, further work may explore how changes in the data alter the reconstructions. For example, the effects of removing observations or adding new data types on the posterior distributions could be addressed with a simple simulation study. The sensitivity of the reconstruction algorithm to data availability can be dealt with similarly, or by using multiple fires as case studies.

In closing, this method of growth curve reconstruction offers a natural way of integrating

prior knowledge and growth data from multiple sources to obtain a best estimate of a wildfire growth curve. Data quality issues are handled elegantly, modeling missing and erroneous data in a way that does not discard potentially useful information. The non-stationary growth curves provided good descriptions of satellite and ground based observations, and was apparently robust to substitutions in the prior distributions. The framework is flexible and can be modified to address a variety of research and management needs. Hence, in light of the data quality issues associated with wildfire growth data, and the benefits of the state space approach, it is recommend that this framework is used as a data reconciliation tool in the analysis of wildfire growth curves.

3.7 REFERENCES

Alexander ME, Thomas DA (2003) Wildland fire behavior case studies and analyses: Other examples, methods, reporting standards, and some practical advice. Fire Management Today, 63:4-12

Andrews P, Finney MA, Fischetti M (2007) Predicting wildfires. Scientific American, 297:46-55

Beverton RJ, Holt SJ (2012) On the dynamics of exploited fish populations (Vol. 11). Springer Science & Business Media.

Birch DS, Morgan P, Kolden CA, Hudak AT, Smith AM (2014) Is proportion burned severely related to daily area burned?. Environmental Research Letters, 9: 064011

Billmire M, French NH, Loboda T, Owen RC, Tyner M (2014) Santa Ana winds and predictors of wildfire progression in southern California. International Journal of Wildland Fire, 23:1119-1129

Brooks SP, Gelman A (1998) General methods for monitoring convergence of iterative simulations. Journal of Computational and Graphical Statistics, 7:434-455

Calkin D, Katuwahl H, Hand M, Holmes T (2014) The effectiveness of suppression resources in large fire management in the US: a review. Advances in Forest Fire Research. doi:10316.2/34013

Carlin, BP, Gelfand AE, Smith AFM (1992) Hierarchical Bayesian analysis of changepoint problems. Applied Statistics. 41:389-405

De La Sen M (2008) The generalized Beverton-Holt equation and the control of populations. Applied Mathematical Modeling. 32: 2312-2328

Finney MA, Grenfell IC, McHugh CW (2009) Modeling containment of large wildfires using generalized linear mixed-model analysis. Forest Science, 55:249-255

Friedman, J., Hastie, T., & Tibshirani, R. (2001). The elements of statistical learning (Vol. 1). Springer, Berlin: Springer series in statistics.

Gelman A, Shirley K (2011). Inference from simulations and monitoring convergence. Handbook of Markov chain Monte Carlo, 163-174

Godsill SJ, Doucet A, West M (2012) Monte Carlo smoothing for nonlinear time series. Journal of the American Statistical Association. doi:10.1198/016214504000000151

Kasischke ES, Williams D, Barry D (2002) Analysis of the patterns of large fires in the boreal forest region of Alaska. International Journal of Wildland Fire, 11:131-144

Kass RE, Raftery AE (1995) Bayes factors. Journal of the American Statistical Association, 90: 773-795

Kolden CA,Weisberg PJ (2007) Assessing accuracy of manually-mapped wildfire perimeters in topographically dissected areas. Fire Ecology. 3:22-31

Li Z, Nadon S, Cihlar J (2000) Satellite-based detection of Canadian boreal forest fires: Development and application of the algorithm. International Journal of Remote Sensing, 21:3057-3069

Mangeon, S, Field R, Fromm M, McHugh C, Voulgarakis A (2015) Satellite versus ground-based estimates of burned area: A comparison between MODIS based burned area and fire agency reports over North America in 2007. The Anthropocene Review. doi:10.1177/2053019615588790

May RM (1976) Simple mathematical models with very complicated dynamics. Nature. 261:459-467

Moeltner K, Kim MK, Zhu E, Yang W (2013). Wildfire smoke and health impacts: A closer look at fire attributes and their marginal effects. Journal of Environmental Economics and Management, 66(3), 476-496

Nakai M, Ke W (2011) Review of the methods for handling missing data in longitudinal data analysis. International Journal of Mathematical Analysis. 5:1-13

Neal RM (2011). MCMC using Hamiltonian dynamics. Handbook of Markov Chain Monte Carlo, 2, 113-162

Parks SA (2014) Mapping day-of-burning with coarse-resolution satellite fire-detection data. International Journal of Wildland fire. 23:215-223

R Development Core Team (2008) R: A Language and Environment for Statistical Computing. Available at: http://www.R-project.org

Raffuse SM, Pryden DA, Sullivan DC, Larkin NK, Strand T, Solomon R (2009) SMARTFIRE algorithm description. US Environmental Protection Agency, Research Triangle Park, NC, by Sonoma Technology, Inc., Petaluma, CA, and the US Forest Service, AirFire Team, Pacific Northwest Research Laboratory, Seattle, WA STI-905517-3719

Roman-Cuesta RM, Gracia M, Retana J (2009) Factors influencing the formation of unburned forest islands within the perimeter of a large forest fire. Forest Ecology and Management, 258:71-80

Short KC (2014) A spatial database of wildfires in the United States, 1992-2011. Earth System Science Data 6:1-27

Taylor SW, Woolford DG, Dean CB, Martell DL (2013) Wildfire prediction to inform fire management: statistical science challenges. Statistical Science. 28:586-615

Tansey K, Beston J, Hoscilo A, Page SE, Paredes Hernández CU (2008) Relationship between

MODIS fire hot spot count and burned area in a degraded tropical peat swamp forest in Central Kalimantan, Indonesia. Journal of Geophysical Research: Atmospheres. 113(D23)

Thompson MP (2013) Modeling Wildfire Incident Complexity Dynamics. PLoS ONE 8: e63297. doi:10.1371/journal.pone.0063297

Turner MG, Hargrove WW, Gardner RH, Romme WH (1994) Effects of fire on landscape heterogeneity in Yellowstone National Park, Wyoming. Journal of Vegetation Science, 5:731-742

Turetsky, M. R., Amiro, B. D., Bosch, E., & Bhatti, J. S. (2004). Historical burn area in western Canadian peatlands and its relationship to fire weather indices. Global Biogeochemical Cycles, 18(4)

Turquety S, Logan JA, Jacob DJ, Hudman RC, Leung FY, Heald CL et al. (2007). Inventory of boreal fire emissions for North America in 2004: Importance of peat burning and pyroconvective injection. Journal of Geophysical Research: Atmospheres. 112(D12)

Veraverbeke S, Sedano F, Hook SJ, Randerson JT, Jin Y, Rogers BM (2014) Mapping the daily progression of large wildland fires using MODIS active fire data. International Journal of Wildland Fire, 23:655-667

Veraverbeke S, Rogers BM, Randerson JT (2015) Daily burned area and carbon emissions from boreal fires in Alaska. Biogeosciences. 12. doi: 10.5194/bg-12-3579-2015

Williams, T. M., Williams, B. J., & Song, B. (2014). Modeling a historic forest fire using GIS and FARSITE. Mathematical & Computational Forestry & Natural Resource Sciences, 6(2)

Walters SP, Schneider NJ, Guthrie JD (2011) Geospatial Multi-Agency Coordination (GeoMAC)

wildland fire perimeters, 2008: U.S. Geological Survey Data Series 612, 6 p.

Zhang, X., Kondragunta, S., & Quayle, B. (2011). Estimation of biomass burned areas using multiple-satellite-observed active fires. IEEE Transactions on Geoscience and Remote Sensing, *49*(11), 4469-4482

Chapter 4. CONCLUSIONS

The research presented in this manuscript serves as a framework that others may build on to further understand how wildfires evolve and grow through time. The results augment a relatively limited existing body of research describing the complexity of wildfire behaviors and their interactions with environment. Theoretical physics-based models of wildfire behavior are popular methods of describing patterns and trends in wildfire activity, as statistical modeling can be challenging for a variety of reasons. Data availability, poor data quality, and limited guidance concerning the quantitative analysis of wildfire growth curves are significant obstacles to modeling wildfire behaviors. However, a number of results and techniques described in this manuscript address these problems, reveal complex relationships between wildfire behavior and the environment, and motivate future areas of research. The cumulative burn area decomposition techniques were particularly important and were used throughout this manuscript to summarize wildfire growth curves using four important growth measurements. Final burn area, peak growth, lag period and containment period represented unique aspects of a wildfire growth that were directly interpretable based on daily burn area time series.

Statistical models of the four growth measurements and two wildfire activity indexes were constructed based on environmental covariates. The models were used to identify regionally important relationships and describe intra-annual changes in wildfire behavior. The models suggested that the drivers of wildfire behaviors were highly complex. Wildfire behavior in nearby regions may be driven by unique weather and landscape variables, and the environmental influences could also change across growth measures. For example, the variables that control wildfire growth were not always the same as those that control final burn area, even within the same region. This complexity was also reflected in the predictive performance, which

varied across regions and growth measurements. Most of the models of wildfire behavior generalized well to independent data, and historical predictions often matched reports of peak wildfire season. Hence, many of the models and results have the potential to be used in a number of applications. Well-validated models can be cautiously applied to climatological data to predict past and future trends in wildfire behaviors. The regionally important predictors of wildfire activity can be used to validate currently existing wildfire risk assessment tools, and provide guidance in constructing new ones. Expected relationships between wildfire behavior and the environment, notably precipitation, can also be verified using the results of this research. This work can be extended to other datasets and the predictive performance potentially improved by including other environmental covariates such as atmospheric stability, fuels and suppression activities, or by using predictions from multiple models.

The four growth measures that captured important characteristics were also used to construct post-hoc reconstructions of the cumulative burn area time series. The presented methods ranged in complexity from simple methods that directly calculate the growth measurements from individual CBA time series to Bayesian state space models that reconstruct realistic growth curves from multiple, corrupted CBA time series. The latter approach was detailed in this manuscript and provided a general tool for researchers and fire managers working with cumulative burn area time series. The models were well suited to address the data quality challenges that are common to growth data and could be modified for a variety of applications including post-hoc burn area reconstruction, forecasting, correlating with environmental covariates, and identification of key growth events. Given the challenges of burn area data, as well as their broad importance to researchers and fire managers, the reconstruction models presented are a promising and robust method of efficiently using growth data to produce realistic

growth curve predictions. The sensitivity of the reconstruction frameworks should be further scrutinized, exploring how changes in the various model components and data alters the model output. Additionally, reducing the sometimes-high computational costs of the reconstruction algorithm would make the model more broadly accessible.

In closing, the results described in this manuscript are of broad importance to wildfire research and have provided details about fire growth that have seldom been explored in the past. The results have described how wildfire behaviors vary over space, and are influenced by unique environmental covariates. Moreover, the manuscript has provided tools and techniques for analyzing cumulative burn area time series that can be used for a variety of applications in research and fire management.

APPENDIX A

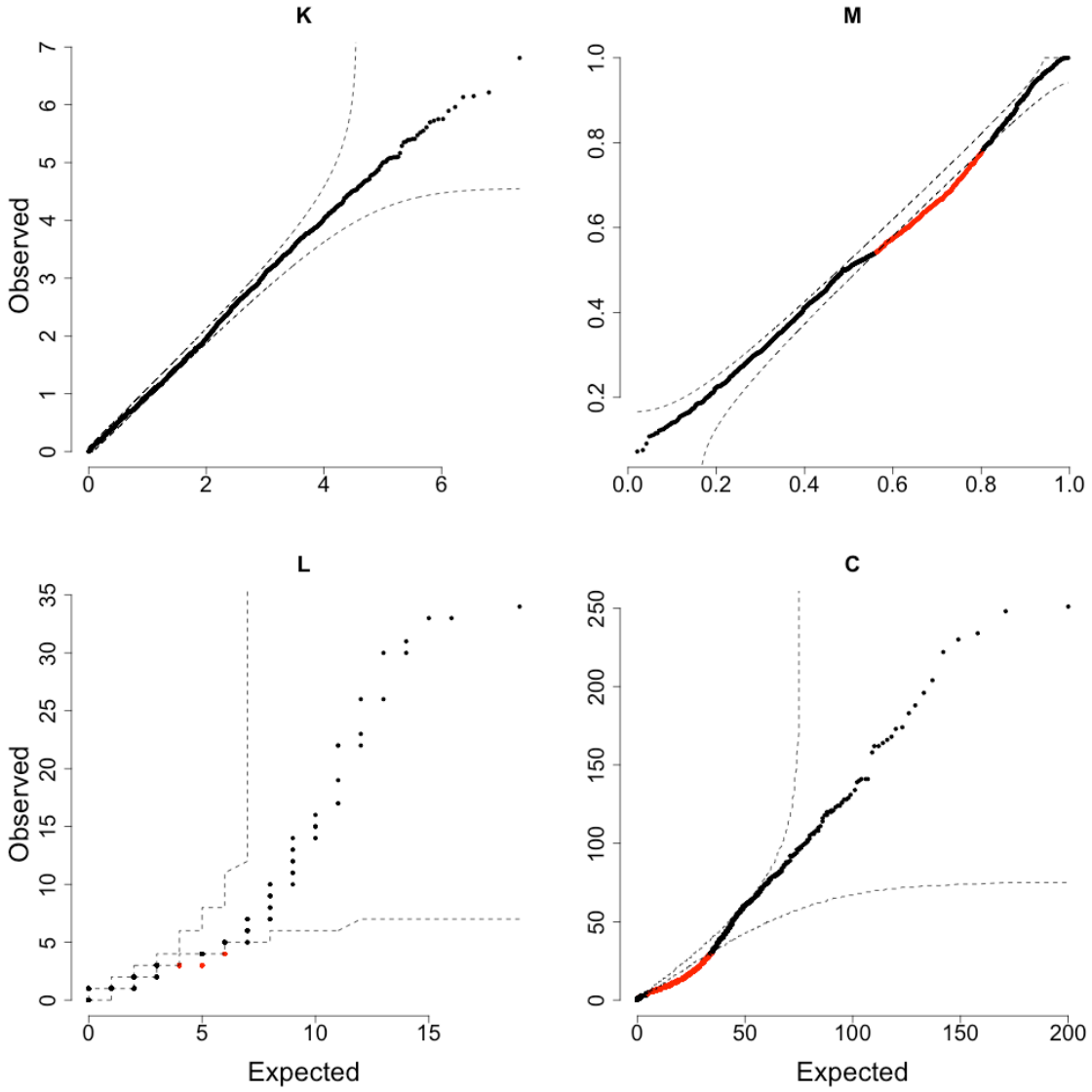

Figure A.1 QQ-plot of the four growth measurements taken from 2,013 fires compared to MLE probability distributions. 95% simultaneous confidence band of MLE distribution is shown with dashed line. Observations that fall outside the confidence band are colored red. Final burn area is described using a generalized gamma distribution.

APPENDIX B

Table B.1 Stationary model JAGS code.

```
model {
#1.)Initial inherent growth parameter.
max.size~dbeta(2.37473644,1.64579462);
r<-pow((max.size+1)/(1-max.size),2);
LR<-log(r);

#2.) Initial conditions.
instant.spike<-pow(1+pow(r,0.5),-1);
last.spike<-pow(1+pow(r,N-1.5),-1);
x0~dunif(last.spike,instant.spike);

#3.) Regression error priors
min.pos.sigma<-3.219013*pow(10,-7);
max.pos.sigma<-1.17481;#Pr(X>10*x)==0.975
sigma ~ dunif(min.pos.sigma,max.pos.sigma);
tau <- pow(sigma,-2);

#4.) Final burn area
LK~dgen.gamma(0.3956239,0.2980782,2.356555);
K<-1000*exp(LK);

# Initialize process and observation equations.
X[1] <- x0;
Y[1] ~ dlnorm(log(K*X[1]), tau);
Z[1] ~ dlnorm(log(X[1]),tau);
for(i in 2:N) {
    #Advance process state equations.
    log(X[i]) <- log(r)+log(X[i-1])-log(X[i-1]*(r-1)+1);
    V[i]<-tau*(X[i-1]/X[i]);#Error on entry i.

    #GeoMac observations.
    Y[i] ~ dlnorm(log(K*X[i]), V[i]);

    #HMS observations.
    Z[i] ~ dlnorm(log(X[i]),V[i]);
}
}
```

APPENDIX C

Table C.1 Non-stationary model JAGS code.

```
model {
        #1.)Inherent growth parameter.
         max.size~dbeta(2.37473644,1.64579462);
         r<-pow((max.size+1)/(1-max.size),2);
         LR<-log(r);

         #2.) Initial conditions.
         instant.spike<-pow(1+pow(r,0.5),-1);
         last.spike<-pow(1+pow(r,N-1.5),-1);
         x0~dunif(last.spike,instant.spike);

         #3.) Regression error priors
         min.pos.sigma<-3.219013*pow(10,-7);
         max.pos.sigma<-1.17481;#Pr(X>10*x)==0.975
         sigma ~ dunif(min.pos.sigma,max.pos.sigma);
         tau <- pow(sigma,-2);

         #4.) Final burn area
         LK~dgen.gamma(0.3956239,0.2980782,2.356555);
         K<-1000*exp(LK);

         #5.) Process error.
         tau.pro~dlnorm(-6.827384,pow(5.21431,-2));

         #Generate multiplicative white noise
         B[1]<-r;
         for(j in 1:(N-1)){
           P[j] ~ dnorm(0,1);
         }

         #Force sample variance to tau.pro
         for(k in 1:(N-1)){
           W[k] <- exp(tau.pro*(P[k]-mean(P))*pow(sd(P),-1));
         }
         W[N]<-1;

         #Initialize process and observation equations.
         X[1] <- x0;# Initialize.
         Y[1] ~ dlnorm(log(K*X[1]), tau)
         Z[1] ~ dlnorm(log(X[1]),tau);
         for(i in 2:N) {
               B[i] <- (r-1)*W[i]+1;#M.W.N.
               log(X[i]) <- log(B[i-1])+log(X[i-1])-log(X[i-1]*(B[i-1]-1)+1);
```

```
            V[i]<-tau*(X[i-1]/X[i]);

            #GeoMac observations.
            Y[i] ~ dlnorm(log(K*X[i]), V[i]); # Observation variation

            #HMS observations.
            Z[i] ~ dlnorm(log(X[i]),V[i]);
        }
}
```